Eur. J. Mech. B - Fluids 20 (2001) 87–126

S0997-7546(00)00133-3/FLA

Shock-wave structure for a binary gas mixture: finite-difference analysis of the Boltzmann equation for hard-sphere molecules

Shingo Kosuge, Kazuo Aoki *, Shigeru Takata

Department of Aeronautics and Astronautics, Graduate School of Engineering, Kyoto University, Kyoto 606-8501, Japan

(Received 17 December 1999; revised 4 March 2000; accepted 12 April 2000)

Abstract – The structure of a normal shock wave for a binary mixture of hard-sphere gases is analyzed numerically on the basis of the Boltzmann equation by a finite-difference method. In the analysis, the complicated collision integrals are computed efficiently as well as accurately by means of the numerical kernel method, which is the generalization to the case of a binary mixture of the method devised by Ohwada in 1993 in the shock-structure analysis for a single-component gas. The transition from the upstream to the downstream uniform state is clarified not only for the macroscopic quantities but also for the velocity distribution functions. © 2001 Éditions scientifiques et médicales Elsevier SAS

shock wave structure / binary gas mixture / Boltzmann equation / kinetic theory of gases / rarefied gas flows

1. Introduction

The analysis of the structure of a normal shock wave in a single component gas is one of the classical problems in modern kinetic theory and has been tackled by various methods, including moment methods (Mott-Smith [1]), model Boltzmann equations (Liepmann et al. [2]), and the direct simulation Monte Carlo (DSMC) method (Bird [3]), since the beginning of 1950's (see, e.g., Cercignani [4], Fiszdon [5], Bird [6], Cercignani et al. [7], and their references). However, an accurate numerical result by means of a finite-difference (or discrete-ordinate) analysis of the Boltzmann equation was reported only in 1993 (Ohwada [8]).

The main difficulty in analyzing the Boltzmann equation by a finite-difference method is to perform accurate computations of the complicated collision integrals. In 1989, Sone and coworkers (Sone et al. [9]) proposed an accurate and efficient method (numerical kernel method) for computing the collision integrals of the linearized Boltzmann equation for hard-sphere molecules. The method has been successfully applied to the finite-difference analyses of various fundamental problems of rarefied gas dynamics, such as the Knudsen-layer problems (Sone et al. [9], Ohwada et al. [10], Ohwada and Sone [11]), plane Poiseuille flow and thermal transpiration (Ohwada et al. [12]), plane Couette flow (Sone et al. [13]), uniform flows past a sphere (Takata et al. [14], Sone et al. [15]), and thermophoresis (Takata and Sone [16]), and the results to be regarded as the standards for these problems have been established. Subsequently, a similar method was developed for the nonlinear Boltzmann equation by Ohwada in the above-mentioned work on the shock-wave structure (Ohwada [8,17]), in which an accurate numerical result was obtained for relatively weak to moderately strong shock waves. The method has also been applied to the analysis of heat transfer between parallel plates (Ohwada [18,19]).

The problem of shock-wave structure for a binary gas mixture has also been a popular subject and has been investigated experimentally (Center [20], Harnett and Muntz [21], Gmurczyk et al. [22]) as well as theoretically.

* Correspondence and reprints.
E-mail address: kaoki@ip.media.kyoto-u.ac.jp (K. Aoki).

The latter approach includes approximate analyses based on moment methods (Oberai [23], Oberai and Sinha [24]) and fluid-dynamic models (Beylich [25], Fernández-Feria and Fernández de la Mora [26]) and numerical analyses based on kinetic models (Abe and Oguchi [27], Hamel [28]) and the DSMC method (Bird [29,30]). (See also Bird [6] and the references therein.) In the present study, we try to extend the method of Ohwada [8] to the case of a binary mixture of hard-sphere gases and investigate the structure of a normal shock wave for the mixture by an accurate finite-difference analysis of the Boltzmann equation. Our aim is to establish the result that can be the standard for the problem. It should be mentioned that a numerical result by another direct method was reported recently (Raines [31]). However, only one case of a rather weak shock is analyzed, and no information is given about the size and accuracy of the computation.

2. Problem and basic equations

2.1. The problem

We consider a steady flow of a binary gas mixture (say, the mixture of A-component and B-component) through a standing normal shock wave. Let us take the X_1 axis of the space coordinates X_i in the direction of the flow. The mixture is in a uniform equilibrium state with speed U_-, temperature T_-, and molecular number densities n_-^A (A-component) and n_-^B (B-component) at upstream infinity ($X_1 = -\infty$), whereas it is in another equilibrium state with speed U_+, temperature T_+, and molecular number densities n_+^A (A-component) and n_+^B (B-component) at downstream infinity ($X_1 = \infty$). The conservations of the molecular number of each component, the total momentum, and the total energy lead to the expressions of the downstream parameters in terms of the upstream ones (the Rankine–Hugoniot relation), which can be arranged in the following form:

$$\frac{n_+^\alpha}{n_-^\alpha} = \frac{4M_-^2}{M_-^2+3} \quad (\alpha = A, B), \tag{1a}$$

$$\frac{U_+}{U_-} = \frac{M_-^2+3}{4M_-^2}, \tag{1b}$$

$$\frac{T_+}{T_-} = \frac{(5M_-^2-1)(M_-^2+3)}{16M_-^2}. \tag{1c}$$

Here M_- is the Mach number at upstream infinity defined by

$$M_- = U_-/(5R_-T_-/3)^{1/2}, \tag{2a}$$

$$R_- = k/\left(m^A\chi_-^A + m^B\chi_-^B\right), \tag{2b}$$

where k is the Boltzmann constant, m^A the mass of a molecule of the A-component, and m^B that of the B-component; χ_-^A and χ_-^B are the concentrations of the A-component and the B-component at upstream infinity, i.e.,

$$\chi_-^\alpha = n_-^\alpha/n_- \quad (\alpha = A, B), \tag{3a}$$

$$n_- = n_-^A + n_-^B. \tag{3b}$$

It is seen from equation (1a) that the concentration of each component at downstream infinity, $\chi_+^\alpha = n_+^\alpha/n_+$ ($n_+ = n_+^A + n_+^B$), is the same as χ_-^α. Therefore, the Mach number at downstream infinity is given by $M_+ = U_+/(5R_-T_+/3)^{1/2}$ and is expressed as

$$M_+ = \left(\frac{M_-^2+3}{5M_-^2-1}\right)^{1/2}, \tag{4}$$

with the aid of equations (1b)–(2a).

We investigate the transition from the upstream to the downstream state through the shock wave on the basis of the Boltzmann equation for a binary mixture under the assumption that the molecules of each component are hard (or rigid) spheres.

2.2. Basic equations

Let ξ_i (or $\boldsymbol{\xi}$) be the molecular velocity, $F^A(X_1, \boldsymbol{\xi})$ the velocity distribution function of the molecules of the A-component, and $F^B(X_1, \boldsymbol{\xi})$ that of the B-component. The Boltzmann equation in the present problem is written in the following form (Kogan [32], Chapman and Cowling [33]).

$$\xi_1 \frac{\partial F^\alpha}{\partial X_1} = \sum_{\beta=A,B} \left\{ G^{\beta\alpha}\left[F^\beta, F^\alpha\right] - \nu^{\beta\alpha}\left[F^\beta\right] F^\alpha \right\} \quad (\alpha = A, B), \tag{5}$$

where

$$G^{\beta\alpha}[f, g] = \frac{(d_m^{\beta\alpha})^2}{2} \int f\left(X_1, \boldsymbol{\xi}_*^{\beta\alpha}\right) g\left(X_1, \boldsymbol{\xi}^{\beta\alpha}\right) |\boldsymbol{a} \cdot \boldsymbol{V}| \, \mathrm{d}\Omega(\boldsymbol{a}) \, \mathrm{d}\boldsymbol{\xi}_*, \tag{6}$$

$$\nu^{\beta\alpha}[f] = \frac{(d_m^{\beta\alpha})^2}{2} \int f(X_1, \boldsymbol{\xi}_*) |\boldsymbol{a} \cdot \boldsymbol{V}| \, \mathrm{d}\Omega(\boldsymbol{a}) \, \mathrm{d}\boldsymbol{\xi}_*, \tag{7}$$

$$\boldsymbol{\xi}^{\beta\alpha} = \boldsymbol{\xi} + \frac{\mu^{\beta\alpha}}{m^\alpha}(\boldsymbol{a} \cdot \boldsymbol{V})\boldsymbol{a}, \qquad \boldsymbol{\xi}_*^{\beta\alpha} = \boldsymbol{\xi}_* - \frac{\mu^{\beta\alpha}}{m^\beta}(\boldsymbol{a} \cdot \boldsymbol{V})\boldsymbol{a}, \quad \boldsymbol{V} = \boldsymbol{\xi}_* - \boldsymbol{\xi}, \tag{8}$$

$$d_m^{\beta\alpha} = \left(d_m^\alpha + d_m^\beta\right)/2, \qquad \mu^{\beta\alpha} = 2m^\alpha m^\beta / \left(m^\alpha + m^\beta\right). \tag{9}$$

Here, d_m^A and d_m^B are the diameter of a molecule of the A-component and that of the B-component, respectively; $\boldsymbol{\xi}_*$ is the integration variable for $\boldsymbol{\xi}$, $\boldsymbol{a}$ is a unit vector, $\mathrm{d}\boldsymbol{\xi}_* = \mathrm{d}\xi_{*1}\,\mathrm{d}\xi_{*2}\,\mathrm{d}\xi_{*3}$, and $\mathrm{d}\Omega(\boldsymbol{a})$ is the solid-angle element around $\boldsymbol{a}$; the domain of integration is the whole space of $\boldsymbol{\xi}_*$ and all directions of $\boldsymbol{a}$.

The boundary condition at upstream infinity is

$$F^\alpha \to n_-^\alpha \left(\frac{m^\alpha}{2\pi k T_-}\right)^{3/2} \exp\left(-\frac{m^\alpha[(\xi_1 - U_-)^2 + \xi_2^2 + \xi_3^2]}{2kT_-}\right), \quad \text{for } \xi_1 > 0 \text{ as } X_1 \to -\infty, \tag{10}$$

and that at downstream infinity is

$$F^\alpha \to n_+^\alpha \left(\frac{m^\alpha}{2\pi k T_+}\right)^{3/2} \exp\left(-\frac{m^\alpha[(\xi_1 - U_+)^2 + \xi_2^2 + \xi_3^2]}{2kT_+}\right), \quad \text{for } \xi_1 < 0 \text{ as } X_1 \to \infty, \tag{11}$$

with $\alpha = A$ and B.

Let n^α be the molecular number density, v_i^α the flow velocity, p^α the pressure, and T^α the temperature of α-component ($\alpha = A, B$), and let n be the molecular number density, ρ the density, v_i the flow velocity, p the pressure, and T the temperature of the total mixture. Then these macroscopic variables are defined as the moments of the velocity distribution functions as follows:

$$\begin{aligned} &n^\alpha = \int F^\alpha \, \mathrm{d}\boldsymbol{\xi}, \qquad v_i^\alpha = \left(1/n^\alpha\right) \int \xi_i F^\alpha \, \mathrm{d}\boldsymbol{\xi}, \\ &p^\alpha = k n^\alpha T^\alpha = (1/3) \int m^\alpha \left(\xi_i - v_i^\alpha\right)^2 F^\alpha \, \mathrm{d}\boldsymbol{\xi}, \end{aligned} \tag{12}$$

$$n=\int\sum_{\alpha=A,B}F^\alpha\,\mathrm{d}\boldsymbol{\xi}=\sum_{\alpha=A,B}n^\alpha,\qquad \rho=\int\sum_{\alpha=A,B}m^\alpha F^\alpha\,\mathrm{d}\boldsymbol{\xi}=\sum_{\alpha=A,B}m^\alpha n^\alpha,$$
$$v_i=\frac{1}{\rho}\int\xi_i\sum_{\alpha=A,B}m^\alpha F^\alpha\,\mathrm{d}\boldsymbol{\xi}=\frac{1}{\rho}\sum_{\alpha=A,B}m^\alpha n^\alpha v_i^\alpha, \tag{13}$$
$$p=knT=\frac{1}{3}\int(\xi_i-v_i)^2\sum_{\alpha=A,B}m^\alpha F^\alpha\,\mathrm{d}\boldsymbol{\xi}=\sum_{\alpha=A,B}\left[p^\alpha+m^\alpha n^\alpha\left(v_i^\alpha-v_i\right)^2/3\right],$$

where $\mathrm{d}\boldsymbol{\xi}=\mathrm{d}\xi_1\,\mathrm{d}\xi_2\,\mathrm{d}\xi_3$, and the integration with respect to $\boldsymbol{\xi}$ in equations (12) and (13) extends to the whole space of $\boldsymbol{\xi}$. In the present problem, the X_2 and X_3 components of the flow velocities vanish, i.e., $v_i^\alpha=v_i=0$ $(i=2,3)$ (see the first paragraph of section 3.2). It should be noted here that, in the literature, the pressure and temperature of each component are often defined in a different way, i.e., by the last equation of (12) with v_i^α replaced by v_i. For this definition, the relation $p=p^A+p^B$ (Dalton's law) holds instead of the expression in the last equation of (13).

2.3. Dimensionless form

We now introduce the following dimensionless variables.

$$x_1=X_1/l_-,\qquad \zeta_i=\xi_i/\left(2kT_-/m^A\right)^{1/2}, \tag{14a}$$
$$\hat{F}^\alpha=F^\alpha\left(2kT_-/m^A\right)^{3/2}/n_-, \tag{14b}$$

where l_- is the mean free path of the molecules of the A-component when it is in an equilibrium state at rest with molecular number density n_- (equation (3b)), i.e.,

$$l_-=\left[\sqrt{2}\pi\left(d_m^A\right)^2 n_-\right]^{-1}. \tag{15}$$

(Note that l_- is independent of the temperature of the equilibrium state for hard-sphere molecules.) In what follows, the symbol $\boldsymbol{\zeta}$ is also used for ζ_i. Then the Boltzmann equation (5) is recast to the following dimensionless form:

$$\zeta_1\frac{\partial\hat{F}^\alpha}{\partial x_1}=\sum_{\beta=A,B}C^{\beta\alpha}\left\{\hat{G}^{\beta\alpha}\left[\hat{F}^\beta,\hat{F}^\alpha\right]-\hat{\nu}\left[\hat{F}^\beta\right]\hat{F}^\alpha\right\}\quad(\alpha=A,B), \tag{16}$$

where

$$\hat{G}^{\beta\alpha}[f,g]=\frac{1}{2\sqrt{2}\pi}\int f\left(x_1,\boldsymbol{\zeta}_*^{\beta\alpha}\right)g\left(x_1,\boldsymbol{\zeta}^{\beta\alpha}\right)|\boldsymbol{a}\cdot\hat{\boldsymbol{V}}|\,\mathrm{d}\Omega(\boldsymbol{a})\,\mathrm{d}\boldsymbol{\zeta}_*, \tag{17}$$
$$\hat{\nu}[f]=\frac{1}{2\sqrt{2}\pi}\int f\left(x_1,\boldsymbol{\zeta}_*\right)|\boldsymbol{a}\cdot\hat{\boldsymbol{V}}|\,\mathrm{d}\Omega(\boldsymbol{a})\,\mathrm{d}\boldsymbol{\zeta}_*, \tag{18}$$
$$\boldsymbol{\zeta}^{\beta\alpha}=\boldsymbol{\zeta}+\frac{\hat{\mu}^{\beta\alpha}}{\hat{m}^\alpha}(\boldsymbol{a}\cdot\hat{\boldsymbol{V}})\boldsymbol{a},\qquad \boldsymbol{\zeta}_*^{\beta\alpha}=\boldsymbol{\zeta}_*-\frac{\hat{\mu}^{\beta\alpha}}{\hat{m}^\beta}(\boldsymbol{a}\cdot\hat{\boldsymbol{V}})\boldsymbol{a},\quad \hat{\boldsymbol{V}}=\boldsymbol{\zeta}_*-\boldsymbol{\zeta}, \tag{19}$$
$$C^{\beta\alpha}=\left(d_m^{\beta\alpha}/d_m^A\right)^2,\qquad \hat{\mu}^{\beta\alpha}=2\hat{m}^\alpha\hat{m}^\beta/\left(\hat{m}^\alpha+\hat{m}^\beta\right),\qquad \hat{m}^\alpha=m^\alpha/m^A. \tag{20}$$

Here, $\boldsymbol{\zeta}_*$ is the integration variable for $\boldsymbol{\zeta}$, and $\mathrm{d}\boldsymbol{\zeta}_*=\mathrm{d}\zeta_{*1}\,\mathrm{d}\zeta_{*2}\,\mathrm{d}\zeta_{*3}$; the domain of integration is the whole space of $\boldsymbol{\zeta}_*$ and all directions of $\boldsymbol{a}$. The corresponding dimensionless forms of boundary conditions (10) and (11) are, with $\alpha=A,B$,

$$\hat{F}^\alpha \to \left(\frac{\hat{m}^\alpha}{\pi}\right)^{3/2} \chi_-^\alpha \exp\left(-\hat{m}^\alpha\left[\left(\zeta_1 - M_-\sqrt{\frac{5}{6\sum_{\beta=A,B}\hat{m}^\beta\chi_-^\beta}}\right)^2 + \zeta_2^2 + \zeta_3^2\right]\right),$$

$$\text{for } \zeta_1 > 0 \text{ as } x_1 \to -\infty, \tag{21}$$

$$\hat{F}^\alpha \to \left(\frac{\hat{m}^\alpha}{\pi}\right)^{3/2} \chi_-^\alpha \frac{n_+^\alpha}{n_-^\alpha}\left(\frac{T_+}{T_-}\right)^{-3/2}$$

$$\times \exp\left(-\hat{m}^\alpha\left(\frac{T_+}{T_-}\right)^{-1}\left[\left(\zeta_1 - \frac{U_+}{U_-}M_-\sqrt{\frac{5}{6\sum_{\beta=A,B}\hat{m}^\beta\chi_-^\beta}}\right)^2 + \zeta_2^2 + \zeta_3^2\right]\right),$$

$$\text{for } \zeta_1 < 0 \text{ as } x_1 \to \infty, \tag{22}$$

where n_+^α/n_-^α, U_+/U_-, and T_+/T_- are given by equation (1) and are determined by M_-.

Since $\hat{m}^A = 1$, $\hat{m}^B = m^B/m^A$, $C^{AA} = 1$, $C^{AB} = C^{BA} = [1 + (d_m^B/d_m^A)]^2/4$, and $C^{BB} = (d_m^B/d_m^A)^2$, and χ_-^A and χ_-^B are related as $\chi_-^A + \chi_-^B = 1$, it is seen that the boundary-value problem, equations (16), (21), and (22), is characterized by the following four dimensionless parameters:

$$m^B/m^A, \qquad d_m^B/d_m^A, \qquad \chi_-^B, \qquad M_-. \tag{23}$$

We analyze the problem numerically for given values of these parameters.

3. Preliminary analysis

3.1. Further transformation

We first transform equation (17). Let us decompose the relative velocity $\hat{\boldsymbol{V}}$ into the components perpendicular and parallel to $\boldsymbol{a}$, i.e.,

$$\hat{\boldsymbol{V}} = \mathbf{w} + \mathbf{z}, \qquad \mathbf{w} = \hat{\boldsymbol{V}} - (\boldsymbol{a}\cdot\hat{\boldsymbol{V}})\boldsymbol{a}, \qquad \mathbf{z} = (\boldsymbol{a}\cdot\hat{\boldsymbol{V}})\boldsymbol{a}. \tag{24}$$

Then, $\boldsymbol{\zeta}^{\beta\alpha}$ and $\boldsymbol{\zeta}_*^{\beta\alpha}$ are expressed as

$$\boldsymbol{\zeta}^{\beta\alpha} = \boldsymbol{\zeta} + \frac{\hat{\mu}^{\beta\alpha}}{\hat{m}^\alpha}\mathbf{z}, \qquad \boldsymbol{\zeta}_*^{\beta\alpha} = \boldsymbol{\zeta} + \mathbf{w} + \left(1 - \frac{\hat{\mu}^{\beta\alpha}}{\hat{m}^\beta}\right)\mathbf{z}. \tag{25}$$

If we change the integration variables from $(\boldsymbol{a}, \boldsymbol{\zeta}_*)$ to $(\mathbf{w}, \mathbf{z})$ noting that $\boldsymbol{a}$ and $-\boldsymbol{a}$ give the same $\mathbf{w}$ and $\mathbf{z}$, we obtain the following expression for $\hat{G}^{\beta\alpha}[f, g]$:

$$\hat{G}^{\beta\alpha}[f,g] = \frac{1}{\sqrt{2}\pi}\int f\left(\boldsymbol{\zeta} + \mathbf{w} + \left(1 - \frac{\hat{\mu}^{\beta\alpha}}{\hat{m}^\beta}\right)\mathbf{z}\right) g\left(\boldsymbol{\zeta} + \frac{\hat{\mu}^{\beta\alpha}}{\hat{m}^\alpha}\mathbf{z}\right) z^{-1}\,\mathrm{d}S(\mathbf{w})\,\mathrm{d}\mathbf{z}, \tag{26}$$

where $z = |\mathbf{z}|$, $\mathrm{d}\mathbf{z} = \mathrm{d}z_1\,\mathrm{d}z_2\,\mathrm{d}z_3$, and $\mathrm{d}S(\mathbf{w})$ is the surface element, around $\mathbf{w}$, of the plane perpendicular to $\mathbf{z}$; the domain of integration with respect to $\mathbf{w}$ is the whole plane perpendicular to $\mathbf{z}$, and that with respect to $\mathbf{z}$ is its whole space; the argument x_1 in f and g is omitted for simplicity.

On the other hand, the integration with respect to $\boldsymbol{a}$ in equation (18) can be carried out, and we have

$$\hat{\nu}[f] = \frac{1}{\sqrt{2}}\int |\boldsymbol{\zeta}_* - \boldsymbol{\zeta}|\, f(\boldsymbol{\zeta}_*)\,\mathrm{d}\boldsymbol{\zeta}_*, \tag{27}$$

where the argument x_1 in f is also omitted.

3.2. Similarity solution

In the present problem, we seek the solution in the following form:

$$\hat{F}^\alpha = \hat{F}^\alpha(x_1, \zeta_1, \zeta_r), \qquad \zeta_r = \left(\zeta_2^2 + \zeta_3^2\right)^{1/2} \quad (\alpha = A, B). \tag{28}$$

The compatibility of this form of $\hat{F}^\alpha$ with the Boltzmann equation (16) is shown by direct substitution. That is, the left-hand side (LHS) of (16) with (28) is obviously a function of x_1, ζ_1, and ζ_r; on the other hand, its right-hand side (RHS) with (28) is, as will be shown below, also a function of the same variables. (The latter fact is readily seen from the rotational invariance of $\hat{G}^{\beta\alpha}[f, g]$ and $\hat{\nu}[f]$. However, since we need the explicit functional form of the RHS of (16) with (28) for numerical analysis, we derive it below.) It is also obvious that equation (28) is compatible with boundary conditions (21) and (22). It follows immediately from (28) that $v_i^\alpha = v_i = 0$ $(i = 2, 3)$.

Now let $L(\zeta_1, \zeta_r)$ and $M(\zeta_1, \zeta_r)$ be arbitrary functions of ζ_1 and ζ_r (they may, of course, depend on x_1). We first derive, from equation (26), the explicit form of $\hat{G}^{\beta\alpha}[L, M]$. We express $\boldsymbol{\zeta}$ in cylindrical coordinates as

$$\zeta_1 = \zeta_1, \qquad \zeta_2 = \zeta_r \cos\psi, \qquad \zeta_3 = \zeta_r \sin\psi, \tag{29}$$

and $\mathbf{z}$ in spherical polar coordinates as

$$z_1 = z\cos\theta, \qquad z_2 = z\sin\theta\cos\epsilon, \qquad z_3 = z\sin\theta\sin\epsilon. \tag{30}$$

We further introduce two orthogonal unit vectors $\mathbf{e}'$ and $\mathbf{e}''$ on the plane perpendicular to $\mathbf{z}$, i.e.,

$$e_1' = 0, \qquad e_2' = -\sin\epsilon, \qquad e_3' = \cos\epsilon, \tag{31a}$$

$$e_1'' = \sin\theta, \qquad e_2'' = -\cos\theta\cos\epsilon, \qquad e_3'' = -\cos\theta\sin\epsilon, \tag{31b}$$

and decompose $\mathbf{w}$ as

$$\mathbf{w} = w'\mathbf{e}' + w''\mathbf{e}''. \tag{32}$$

Then, noting that $\mathrm{d}S(\mathbf{w}) = \mathrm{d}w'\,\mathrm{d}w''$ and $\mathrm{d}\mathbf{z} = z^2\sin\theta\,\mathrm{d}z\,\mathrm{d}\theta\,\mathrm{d}\epsilon$, we obtain the following expression for $\hat{G}^{\beta\alpha}[L, M]$:

$$\begin{aligned}
\hat{G}^{\beta\alpha}[L, M] &= \frac{1}{\sqrt{2}\pi}\int_0^\pi\int_{-\pi}^{\pi}\int_0^\infty\int_{-\infty}^{\infty}\int_{-\infty}^{\infty}\Delta_G^{\beta\alpha}\left(\zeta_1, \zeta_r, z, \theta, \cos(\epsilon-\psi), \sin(\epsilon-\psi), w', w''\right)\mathrm{d}w'\,\mathrm{d}w''\,\mathrm{d}z\,\mathrm{d}\epsilon\,\mathrm{d}\theta \\
&= \frac{1}{\sqrt{2}\pi}\int_0^\pi\int_{-\pi}^{\pi}\int_0^\infty\int_{-\infty}^{\infty}\int_{-\infty}^{\infty}\Delta_G^{\beta\alpha}(\zeta_1, \zeta_r, z, \theta, \cos\bar{\epsilon}, \sin\bar{\epsilon}, w', w'')\,\mathrm{d}w'\,\mathrm{d}w''\,\mathrm{d}z\,\mathrm{d}\bar{\epsilon}\,\mathrm{d}\theta \\
&= \frac{\sqrt{2}}{\pi}\int_0^\pi\int_0^\pi\int_0^\infty\int_{-\infty}^{\infty}\int_{-\infty}^{\infty}\Delta_G^{\beta\alpha}(\zeta_1, \zeta_r, z, \theta, \cos\bar{\epsilon}, \sin\bar{\epsilon}, w', w'')\,\mathrm{d}w'\,\mathrm{d}w''\,\mathrm{d}z\,\mathrm{d}\bar{\epsilon}\,\mathrm{d}\theta,
\end{aligned} \tag{33}$$

where

$$\Delta_G^{\beta\alpha}(\zeta_1, \zeta_r, z, \theta, \cos\bar{\epsilon}, \sin\bar{\epsilon}, w', w'') = L(J_1, J_r)M(K_1, K_r)z\sin\theta, \tag{34}$$

and

$$J_1 = \zeta_1 + w'' \sin\theta + (1 - \hat{\mu}^{\beta\alpha}/\hat{m}^{\beta}) z \cos\theta, \tag{35a}$$

$$J_r = \{(w' - \zeta_r \sin\bar{\epsilon})^2 + [w'' \cos\theta - \zeta_r \cos\bar{\epsilon} - (1 - \hat{\mu}^{\beta\alpha}/\hat{m}^{\beta}) z \sin\theta]^2\}^{1/2}, \tag{35b}$$

$$K_1 = \zeta_1 + (\hat{\mu}^{\beta\alpha}/\hat{m}^{\alpha}) z \cos\theta, \tag{35c}$$

$$K_r = \{[(\hat{\mu}^{\beta\alpha}/\hat{m}^{\alpha}) z \sin\theta + \zeta_r \cos\bar{\epsilon}]^2 + (\zeta_r \sin\bar{\epsilon})^2\}^{1/2}. \tag{35d}$$

In the last equality of equation (33), the property

$$\Delta_G^{\beta\alpha}(\zeta_1, \zeta_r, z, \theta, \cos(-\bar{\epsilon}), \sin(-\bar{\epsilon}), -w', w'') = \Delta_G^{\beta\alpha}(\zeta_1, \zeta_r, z, \theta, \cos\bar{\epsilon}, \sin\bar{\epsilon}, w', w''), \tag{36}$$

has been used to reduce the range of integration with respect to $\bar{\epsilon}$ to $[0,\ \pi]$.

On the other hand, in equation (27), we express $\boldsymbol{\zeta}_*$ in cylindrical coordinates as

$$\zeta_{*1} = \zeta_{*1}, \qquad \zeta_{*2} = \zeta_{*r} \cos\phi, \qquad \zeta_{*3} = \zeta_{*r} \sin\phi, \tag{37}$$

and use equation (29) for $\boldsymbol{\zeta}$. Then, we obtain the following expression for $\hat{\nu}[L]$:

$$\begin{aligned}\hat{\nu}[L] &= \frac{1}{\sqrt{2}} \int_{-\infty}^{\infty} \int_{0}^{\infty} \int_{-\pi}^{\pi} \Delta_\nu\big(\zeta_1, \zeta_r, \zeta_{*1}, \zeta_{*r}, \cos(\phi - \psi)\big)\, \mathrm{d}\phi\, \mathrm{d}\zeta_{*r}\, \mathrm{d}\zeta_{*1} \\ &= \frac{1}{\sqrt{2}} \int_{-\infty}^{\infty} \int_{0}^{\infty} \int_{-\pi}^{\pi} \Delta_\nu(\zeta_1, \zeta_r, \zeta_{*1}, \zeta_{*r}, \cos\bar{\phi})\, \mathrm{d}\bar{\phi}\, \mathrm{d}\zeta_{*r}\, \mathrm{d}\zeta_{*1},\end{aligned} \tag{38}$$

where

$$\Delta_\nu(\zeta_1, \zeta_r, \zeta_{*1}, \zeta_{*r}, \cos\bar{\phi}) = L(\zeta_{*1}, \zeta_{*r}) \hat{V} \zeta_{*r}, \tag{39a}$$

$$\hat{V} = \big[(\zeta_{*1} - \zeta_1)^2 + \zeta_{*r}^2 + \zeta_r^2 - 2\zeta_{*r}\zeta_r \cos\bar{\phi}\big]^{1/2}. \tag{39b}$$

From equations (33) and (38), it is obvious that the RHS of (16) with (28) is a function of x_1, ζ_1, and ζ_r.

4. Numerical analysis

The method of analysis is the extension of the method developed by Ohwada [8] for a single component gas to the case of a binary mixture. The details will be given below.

4.1. Finite-difference analysis

In this subsection we explain the finite-difference scheme and the solution procedure. In the actual computation, we consider a finite range of x_1, i.e., $-D \leqslant x_1 \leqslant D$, instead of the infinite range and impose the condition (21) at $x_1 = -D$ for $\zeta_1 > 0$ and (22) at $x_1 = D$ for $\zeta_1 < 0$. As for the molecular velocity, we only restrict ζ_1 to a finite range, i.e., $-Z_1^{\alpha} \leqslant \zeta_1 \leqslant Z_1^{\alpha\prime}$ for the α-component ($\alpha = A, B$) (as seen below, we do not need to restrict the range of ζ_r because of our solution method). The constants D, Z_1^{α}, and $Z_1^{\alpha\prime}$ are chosen in such a way that the deviation of the velocity distribution $\hat{F}^{\alpha}$ from the upstream Maxwellian (21) (or from the downstream Maxwellian (22)) is negligibly small at $x_1 \simeq -D$ (or at $x_1 \simeq D$) and that $\hat{F}^{\alpha}$ itself is negligibly small at $\zeta_1 \simeq -Z_1^{\alpha}$ and $\zeta_1 \simeq Z_1^{\alpha\prime}$. The choice is to be validated from the result of numerical computation. Now, let $x_1^{(i)}$ ($i = -N_D, \ldots, 0, \ldots, N_D$) be the lattice points in x_1 ($x_1^{(-N_D)} = -D$, $x_1^{(0)} = 0$, $x_1^{(N_D)} = D$), and let ($\zeta_1^{\alpha(j)}$, $\zeta_r^{\alpha(k)}$) ($j = -N_m^{\alpha}, \ldots, 0, \ldots, N_p^{\alpha}$; $k = 0, 1, \ldots, H^{\alpha}$) be the lattice points in the $\zeta_1\zeta_r$-plane for the α-component

($\zeta_1^{\alpha(-N_m^\alpha)} = -Z_1^\alpha$, $\zeta_1^{\alpha(0)} = 0$, $\zeta_1^{\alpha(N_p^\alpha)} = Z_1^{\alpha\prime}$; $\zeta_r^{\alpha(0)} = 0$; as will be seen in the next subsection, the lattice point $\zeta_r^{\alpha(0)}$ is not used in our practical computation). Then, we define $\hat{F}_i^{\alpha(n)}(\zeta_1, \zeta_r)$ and $\hat{F}_{ijk}^{\alpha(n)}$ as follows:

$$\hat{F}_i^{\alpha(n)}(\zeta_1, \zeta_r) = \hat{F}^\alpha\big(x_1^{(i)}, \zeta_1, \zeta_r\big) \quad \text{at the } n\text{th iteration step}, \tag{40a}$$

$$\hat{F}_{ijk}^{\alpha(n)} = \hat{F}_i^{\alpha(n)}\big(\zeta_1^{\alpha(j)}, \zeta_r^{\alpha(k)}\big). \tag{40b}$$

When confusion is expected, the commas are placed between subscripts as $\hat{F}_{i+1,j,k}^{\alpha(n)}$ in equation (41a) below. The finite-difference scheme that we adopt is essentially the same as that in Ohwada [8], i.e.,

$$\begin{aligned}&\zeta_1^{\alpha(j)}\big(\hat{F}_{i+1,j,k}^{\alpha(n+1)} - \hat{F}_{ijk}^{\alpha(n+1)}\big)\big/\big(x_1^{(i+1)} - x_1^{(i)}\big)\\ &\quad= \sum_{\beta=A,B} C^{\beta\alpha}\big(\hat{G}_{i+1,j,k}^{\beta\alpha(n)} - \hat{\nu}_{i+1,j,k}^{\beta\alpha(n)}\hat{F}_{i+1,j,k}^{\alpha(n+1)} + \hat{G}_{ijk}^{\beta\alpha(n)} - \hat{\nu}_{ijk}^{\beta\alpha(n)}\hat{F}_{ijk}^{\alpha(n+1)}\big)/2 \quad (j > 0),\end{aligned} \tag{41a}$$

$$\begin{aligned}&\zeta_1^{\alpha(j)}\big(\hat{F}_{i-1,j,k}^{\alpha(n+1)} - \hat{F}_{ijk}^{\alpha(n+1)}\big)\big/\big(x_1^{(i-1)} - x_1^{(i)}\big)\\ &\quad= \sum_{\beta=A,B} C^{\beta\alpha}\big(\hat{G}_{i-1,j,k}^{\beta\alpha(n)} - \hat{\nu}_{i-1,j,k}^{\beta\alpha(n)}\hat{F}_{i-1,j,k}^{\alpha(n+1)} + \hat{G}_{ijk}^{\beta\alpha(n)} - \hat{\nu}_{ijk}^{\beta\alpha(n)}\hat{F}_{ijk}^{\alpha(n+1)}\big)/2 \quad (j < 0),\end{aligned} \tag{41b}$$

$$0 = \sum_{\beta=A,B} C^{\beta\alpha}\big(\hat{G}_{ijk}^{\beta\alpha(n)} - \hat{\nu}_{ijk}^{\beta\alpha(n)}\hat{F}_{ijk}^{\alpha(n+1)}\big) \quad (j = 0), \tag{41c}$$

where

$$\hat{G}_{ijk}^{\beta\alpha(n)} = \hat{G}^{\beta\alpha}\big[\hat{F}_i^{\beta(n)}(\zeta_1, \zeta_r), \hat{F}_i^{\alpha(n)}(\zeta_1, \zeta_r)\big] \quad \text{at } (\zeta_1,\ \zeta_r) = \big(\zeta_1^{\alpha(j)},\ \zeta_r^{\alpha(k)}\big), \tag{42a}$$

$$\hat{\nu}_{ijk}^{\beta\alpha(n)} = \hat{\nu}\big[\hat{F}_i^{\beta(n)}(\zeta_1, \zeta_r)\big] \quad \text{at } (\zeta_1,\ \zeta_r) = \big(\zeta_1^{\alpha(j)},\ \zeta_r^{\alpha(k)}\big). \tag{42b}$$

The most complicated part in this scheme is the evaluation of $\hat{G}_{ijk}^{\beta\alpha(n)}$ and $\hat{\nu}_{ijk}^{\beta\alpha(n)}$, which will be explained in the following subsections. With this method for the evaluation, the process of computation for the above finite-difference scheme is obvious. We first choose appropriate initial distributions $\hat{F}_{ijk}^{\alpha(0)}$. Now, suppose that $\hat{F}_{ijk}^{\alpha(n)}$ are known.

(i) Compute $\hat{G}_{ijk}^{\beta\alpha(n)}$ and $\hat{\nu}_{ijk}^{\beta\alpha(n)}$ using $\hat{F}_{ijk}^{\alpha(n)}$.

(ii) For $j > 0$, compute $\hat{F}_{ijk}^{\alpha(n+1)}$ successively from $i = -N_D + 1$ to $i = N_D$ from equation (41a) using $\hat{G}_{ijk}^{\beta\alpha(n)}$, $\hat{\nu}_{ijk}^{\beta\alpha(n)}$ and the boundary condition at $x_1 = -D$.

(iii) For $j < 0$, compute $\hat{F}_{ijk}^{\alpha(n+1)}$ successively from $i = N_D - 1$ to $i = -N_D$ from equation (41b) using $\hat{G}_{ijk}^{\beta\alpha(n)}$, $\hat{\nu}_{ijk}^{\beta\alpha(n)}$ and the boundary condition at $x_1 = D$.

(iv) For $j = 0$, compute $\hat{F}_{i0k}^{\alpha(n+1)}$ for all i from equation (41c) using $\hat{G}_{i0k}^{\beta\alpha(n)}$ and $\hat{\nu}_{i0k}^{\beta\alpha(n)}$.

Repeat the steps (i)–(iv) for $n = 0, 1, \ldots$ until $\hat{F}_{ijk}^{\alpha(n)}$ converges.

4.2. Numerical computation of collision integrals

In order to complete the above finite-difference scheme, we need to express $\hat{G}_{ijk}^{\beta\alpha(n)}$ and $\hat{\nu}_{ijk}^{\beta\alpha(n)}$ in terms of $\hat{F}_{ijk}^{\alpha(n)}$. For this purpose, we first express $\hat{F}_i^{\alpha(n)}(\zeta_1, \zeta_r)$ in terms of $\hat{F}_{ijk}^{\alpha(n)}$. It is done by the following three steps. First, we expand $\hat{F}_i^{\alpha(n)}(\zeta_1, \zeta_r)$ with respect to ζ_1 using a set of basis functions $\Psi_j^\alpha(\zeta_1)$, i.e.,

$$\hat{F}_i^{\alpha(n)}(\zeta_1, \zeta_r) = \sum_{j=-N_m^\alpha}^{N_p^\alpha} \hat{F}_i^{\alpha(n)}\big(\zeta_1^{\alpha(j)}, \zeta_r\big)\Psi_j^\alpha(\zeta_1), \tag{43}$$

where $\Psi_j^\alpha(\zeta_1)$ is assumed to have the following property: $\Psi_j^\alpha(\zeta_1) = 1$ at $\zeta_1 = \zeta_1^{\alpha(j)}$, and $\Psi_j^\alpha(\zeta_1) = 0$ at $\zeta_1 = \zeta_1^{\alpha(l)}$ ($l \neq j$). In the practical computation, we use Ψ_j^α that is nonzero only in a neighborhood (e.g., some lattice intervals) of $\zeta_1 = \zeta_1^{\alpha(j)}$. The explicit choice of Ψ_j^α will be made later. [Hereafter, we assume equation (43) for the whole range of ζ_1; therefore, the practical range of ζ_1 becomes slightly wider than $-Z_1^\alpha \leqslant \zeta_1 \leqslant Z_1^{\alpha\prime}$.] Second, expecting that $\hat{F}_i^{\alpha(n)}$ is a smooth and rapidly decreasing function of $\sqrt{\hat{m}^\alpha}\zeta_r$, we assume the following form of $\hat{F}_i^{\alpha(n)}(\zeta_1^{\alpha(j)}, \zeta_r)$:

$$\hat{F}_i^{\alpha(n)}(\zeta_1^{\alpha(j)}, \zeta_r) = \exp\left(-\frac{\hat{m}^\alpha \zeta_r^2}{2}\right) \sum_{m=0}^{H^\alpha - 1} a_{ijm}^{\alpha(n)} L_m(\hat{m}^\alpha \zeta_r^2), \tag{44}$$

where $L_m(y)$ is the Laguerre polynomial (Abramowitz and Stegun [34]) of mth order, which is defined by

$$L_m(y) = \sum_{s=0}^{m} \frac{(-1)^s}{s!} \binom{m}{s} y^s, \tag{45}$$

and satisfy the relation

$$\int_0^\infty L_m(y) L_n(y) \exp(-y)\, \mathrm{d}y = \delta_{mn}. \tag{46}$$

The system of functions $\exp(-y/2)L_m(y)$ ($m = 0, 1, \ldots$) forms a complete orthonormal system in $L^2(0, \infty)$. Therefore, equation (44) means that, assuming $\hat{F}_i^{\alpha(n)}(\zeta_1^{\alpha(j)}, \zeta_r)$ to be a rapidly decreasing function of $\hat{m}^\alpha \zeta_r^2$, we expand it in terms of the orthonormal system and truncate it at the H^αth term. If we consider equation (44) at the lattice points $\zeta_r = \zeta_r^{\alpha(k)}$ ($k = 1, \ldots, H^\alpha$), we have

$$\hat{F}_{ijk}^{\alpha(n)} = \exp\left(-\frac{\hat{m}^\alpha (\zeta_r^{\alpha(k)})^2}{2}\right) \sum_{m=0}^{H^\alpha - 1} a_{ijm}^{\alpha(n)} L_m\left(\hat{m}^\alpha \left(\zeta_r^{\alpha(k)}\right)^2\right). \tag{47}$$

The coefficients $a_{ijm}^{\alpha(n)}$ ($m = 0, \ldots, H^\alpha - 1$) in (44) are expressed in terms of $\hat{F}_{ijk}^{\alpha(n)}$ ($k = 1, \ldots, H^\alpha$) by solving the system of linear algebraic equations (47). (Equation (44) with $a_{ijm}^{\alpha(n)}$ thus determined is equivalent to approximating $\exp(\hat{m}^\alpha \zeta_r^2/2)\hat{F}_i^{\alpha(n)}(\zeta_1^{\alpha(j)}, \zeta_r)$ by the $H^\alpha - 1$ degree polynomial of $\hat{m}^\alpha \zeta_r^2$ that takes the values $\exp(\hat{m}^\alpha (\zeta_r^{\alpha(k)})^2/2)\hat{F}_{ijk}^{\alpha(n)}$ at $\zeta_r = \zeta_r^{\alpha(k)}$ ($k = 1, \ldots, H^\alpha$) (Lagrange interpolation).) Equation (44), arranged in the form of power series of $\hat{m}^\alpha \zeta_r^2$, can be written as

$$\hat{F}_i^{\alpha(n)}(\zeta_1^{\alpha(j)}, \zeta_r) = \exp\left(-\frac{\hat{m}^\alpha \zeta_r^2}{2}\right) \sum_{m=0}^{H^\alpha - 1} A_{ijm}^{\alpha(n)} \left(\hat{m}^\alpha \zeta_r^2\right)^m, \tag{48}$$

where $A_{ijm}^{\alpha(n)}$ are the constants depending explicitly on $\hat{F}_{ijk}^{\alpha(n)}$ and the lattice points $\zeta_r^{\alpha(k)}$ ($k = 1, \ldots, H^\alpha$) (Explicit expression of $A_{ijm}^{\alpha(n)}$ will be given later for a special choice of $\zeta_r^{\alpha(k)}$). Finally, by substituting (48) into (43), we have the following expression of $\hat{F}_i^{\alpha(n)}(\zeta_1, \zeta_r)$ in terms of $\hat{F}_{ijk}^{\alpha(n)}$:

$$\hat{F}_i^{\alpha(n)}(\zeta_1, \zeta_r) = \exp\left(-\frac{\hat{m}^\alpha \zeta_r^2}{2}\right) \sum_{j=-N_m^\alpha}^{N_p^\alpha} \sum_{m=0}^{H^\alpha - 1} A_{ijm}^{\alpha(n)} \Psi_j^\alpha(\zeta_1) \left(\hat{m}^\alpha \zeta_r^2\right)^m. \tag{49}$$

If we substitute (49) into (42), we obtain the desired expressions of $\hat{G}_{ijk}^{\beta\alpha(n)}$ and $\hat{v}_{ijk}^{\beta\alpha(n)}$, i.e.,

$$\hat{G}_{ijk}^{\beta\alpha(n)} = \sum_{p=-N_m^\beta}^{N_p^\beta} \sum_{q=-N_m^\alpha}^{N_p^\alpha} \sum_{a=0}^{H^\beta-1} \sum_{b=0}^{H^\alpha-1} \Omega_{pqab}^{\beta\alpha jk} A_{ipa}^{\beta(n)} A_{iqb}^{\alpha(n)}, \tag{50a}$$

$$\hat{v}_{ijk}^{\beta\alpha(n)} = \sum_{p=-N_m^\beta}^{N_p^\beta} \sum_{a=0}^{H^\beta-1} \Lambda_{pa}^{\beta\alpha jk} A_{ipa}^{\beta(n)}, \tag{50b}$$

where

$$\Omega_{pqab}^{\beta\alpha jk} = \hat{G}^{\beta\alpha}\left[\Psi_p^\beta(\zeta_1)\left(\hat{m}^\beta \zeta_r^2\right)^a E_r^\beta,\, \Psi_q^\alpha(\zeta_1)\left(\hat{m}^\alpha \zeta_r^2\right)^b E_r^\alpha\right] \quad \text{at } (\zeta_1,\ \zeta_r) = \left(\zeta_1^{\alpha(j)},\ \zeta_r^{\alpha(k)}\right), \tag{51a}$$

$$\Lambda_{pa}^{\beta\alpha jk} = \hat{v}\left[\Psi_p^\beta(\zeta_1)\left(\hat{m}^\beta \zeta_r^2\right)^a E_r^\beta\right] \quad \text{at } (\zeta_1,\ \zeta_r) = \left(\zeta_1^{\alpha(j)},\ \zeta_r^{\alpha(k)}\right), \tag{51b}$$

$$E_r^\alpha = \exp\left(-\hat{m}^\alpha \zeta_r^2/2\right). \tag{51c}$$

The $\Omega_{pqab}^{\beta\alpha jk}$ and $\Lambda_{pa}^{\beta\alpha jk}$ are the universal constants in the sense that they do not depend on i and n. Therefore, we can compute them beforehand once we have chosen the lattice points in the $\zeta_1\zeta_r$-plane and the explicit form of $\Psi_j^\alpha(\zeta_1)$ (note that they depend also on m^B/m^A, but not on d_m^B/d_m^A). We call $\Omega_{pqab}^{\beta\alpha jk}$ and $\Lambda_{pa}^{\beta\alpha jk}$ the 'numerical kernels' of the collision integrals.

In this way, the computation of the collision integrals has been reduced to the matrix products of the numerical kernels and $A_{ijk}^{\alpha(n)}$ that are determined by $\hat{F}_{ijk}^{\alpha(n)}$ and by the lattice points $\zeta_r^{\alpha(k)}$. A convenient choice of $\zeta_r^{\alpha(k)}$ is,

$$\zeta_r^{\alpha(k)} = \sqrt{y_k/\hat{m}^\alpha} \quad (k = 1, \ldots, H), \tag{52}$$

where $H^\alpha = H$ is assumed for simplicity, and y_k stands for the zeros ($y_k < y_l$ for $k < l$) of the Laguerre polynomial $L_H(y)$ of order H. Then, we obtain the following simple expression of the solution $a_{ijm}^{\alpha(n)}$ of the system of algebraic equations (47):

$$a_{ijm}^{\alpha(n)} = \sum_{k=1}^{H} w_{mk} \hat{F}_{ijk}^{\alpha(n)}, \tag{53a}$$

$$w_{mk} = \frac{L_m(y_k)\exp(y_k/2)}{c_{H-1,H-1} L_{H-1}(y_k) \prod_{s=1(\neq k)}^{H} (y_k - y_s)}, \tag{53b}$$

where c_{mn} is the coefficient of y^m in $L_n(y)$ (see appendix A for the derivation of equation (53)). Equation (53a) leads to the concise expression of the coefficients $A_{ijm}^{\alpha(n)}$ in equation (49) in terms of $\hat{F}_{ijk}^{\alpha(n)}$ and y_k (appendix A), i.e.,

$$A_{ijm}^{\alpha(n)} = \sum_{k=1}^{H} \sum_{l=0}^{H-1} M_{ml} w_{lk} \hat{F}_{ijk}^{\alpha(n)}, \tag{54a}$$

$$M_{ml} = \begin{cases} 0 & (m > l), \\ c_{ml} & (0 \leqslant m \leqslant l). \end{cases} \tag{54b}$$

4.3. Numerical kernels of collision integrals

4.3.1. Basis functions

The number of the elements of the numerical kernels $\Omega_{pqab}^{\beta\alpha jk}$ is still too large for precise numerical computations because of its six-fold indices (j, k, p, q, a, b). However, by using a uniform lattice system for ζ_1 that is common to both components, i.e.,

$$\zeta_1^{\alpha(j)} = \zeta_1^{(j)} = jh \quad (j = -N_m, \ldots, 0, \ldots, N_p) \tag{55}$$

(here $N_m^\alpha = N_m$ and $N_p^\alpha = N_p$ are assumed for simplicity), and by exploiting the basic properties of $\hat{G}^{\beta\alpha}$ and $\hat{\nu}$, we can reduce the number of the independent elements of $\Omega_{pqab}^{\beta\alpha jk}$ and $\Lambda_{pa}^{\beta\alpha jk}$ significantly, as we will see below. Since $\hat{F}^\alpha$ is expected to be a rapidly decaying function of $\sqrt{\hat{m}^\alpha}\zeta_1$, it is reasonable to use different lattice systems for individual gas components, such as $\zeta_1^{\alpha(j)} = jh/\sqrt{\hat{m}^\alpha}$, rather than equation (55). But in this case, such reduction of the number of the independent elements is not possible. We can perform much more efficient computation with the lattice system (55).

To define the explicit form of the basis functions $\Psi_j^\alpha(\zeta_1)$ in equation (43), we introduce the following $\widetilde{\Psi}_j(\zeta_1)$:

$$\widetilde{\Psi}_{2\ell}(\zeta_1) = \begin{cases} [\zeta_1 - (2\ell-1)h][\zeta_1 - (2\ell-2)h]/2h^2 & [(2\ell-2)h \leqslant \zeta_1 \leqslant 2\ell h], \\ [\zeta_1 - (2\ell+1)h][\zeta_1 - (2\ell+2)h]/2h^2 & [2\ell h < \zeta_1 \leqslant (2\ell+2)h], \\ 0 & \text{(otherwise)}, \end{cases} \tag{56a}$$

$$\widetilde{\Psi}_{2\ell+1}(\zeta_1) = \begin{cases} -(\zeta_1 - 2\ell h)[\zeta_1 - (2\ell+2)h]/h^2 & [2\ell h \leqslant \zeta_1 \leqslant (2\ell+2)h], \\ 0 & \text{(otherwise)}. \end{cases} \tag{56b}$$

Then, in the computation of $\Omega_{pqab}^{\beta\alpha jk}$ and $\Lambda_{pa}^{\beta\alpha jk}$, we use two different sets of basis functions depending on the parity of j that are common to both components, i.e.,

$$\Psi_p^\alpha(\zeta_1) = \Psi_p(\zeta_1) = \widetilde{\Psi}_p(\zeta_1) \quad (p = 0, \pm1, \pm2, \ldots), \text{ for } j = 2\ell, \tag{57a}$$

$$\Psi_p^\alpha(\zeta_1) = \Psi_p(\zeta_1) = \widetilde{\Psi}_{p-1}(\zeta_1 - h) \quad (p = 0, \pm1, \pm2, \ldots), \text{ for } j = 2\ell + 1. \tag{57b}$$

By this choice of the basis functions, equation (43) means that $\hat{F}_i^{\alpha(n)}(\zeta_1, \zeta_r)$, as the function of ζ_1, is approximated by a piecewise quadratic function of ζ_1 that takes the value $\hat{F}_i^{\alpha(n)}(\zeta_1^{(j)}, \zeta_r)$ at the lattice point $\zeta_1 = \zeta_1^{(j)}$ $(j = -N_m, \ldots, 0, \ldots, N_p)$. The piecewise quadratic function is quadratic in the interval $2\ell h \leqslant \zeta_1 \leqslant 2(\ell+1)h$ for (57a) and in $(2\ell-1)h \leqslant \zeta_1 \leqslant (2\ell+1)h$ for (57b). (These statements are not true in a small neighborhood of the outermost lattice point $\zeta_1^{(-N_m)}$ or $\zeta_1^{(N_p)}$, where the value of $\hat{F}_i^{\alpha(n)}(\zeta_1, \zeta_r)$ is negligibly small.) The use of the two sets of basis functions is just for convenience that the lattice point $\zeta_1^{(j)}$ under consideration in the integrals in equation (51) is always at a node ($\zeta_1^{(2\ell)}$ for (57a) and $\zeta_1^{(2\ell+1)}$ for (57b)) of the piecewise quadratic function. The $\widetilde{\Psi}_p(\zeta_1)$ defined above has the property

$$\widetilde{\Psi}_p\big(\zeta_1 + \zeta_1^{(2\ell)}\big) = \widetilde{\Psi}_p(\zeta_1 + 2\ell h) = \widetilde{\Psi}_{p-2\ell}(\zeta_1), \tag{58a}$$

$$\widetilde{\Psi}_p(-\zeta_1) = \widetilde{\Psi}_{-p}(\zeta_1). \tag{58b}$$

On the other hand, $\hat{G}^{\beta\alpha}$ and $\hat{\nu}$ satisfy the following relations.

$$\hat{G}^{\beta\alpha}\big[f(\boldsymbol{\zeta}), g(\boldsymbol{\zeta})\big](\boldsymbol{\zeta}) = \hat{G}^{\beta\alpha}\big[f(\boldsymbol{\zeta} + \boldsymbol{a}), g(\boldsymbol{\zeta} + \boldsymbol{a})\big](\boldsymbol{\zeta} - \boldsymbol{a}), \tag{59a}$$

$$\hat{\nu}\big[f(\boldsymbol{\zeta})\big](\boldsymbol{\zeta}) = \hat{\nu}\big[f(\boldsymbol{\zeta}+\boldsymbol{a})\big](\boldsymbol{\zeta}-\boldsymbol{a}), \tag{59b}$$

$$\hat{G}^{\beta\alpha}\big[f(\zeta_1,\zeta_r), g(\zeta_1,\zeta_r)\big](0,\zeta_r) = \hat{G}^{\beta\alpha}\big[f(-\zeta_1,\zeta_r), g(-\zeta_1,\zeta_r)\big](0,\zeta_r), \tag{59c}$$

$$\hat{\nu}\big[f(\zeta_1,\zeta_r)\big](0,\zeta_r) = \hat{\nu}\big[f(-\zeta_1,\zeta_r)\big](0,\zeta_r), \tag{59d}$$

$$\hat{G}^{\alpha\alpha}\big[f(\boldsymbol{\zeta}), g(\boldsymbol{\zeta})\big] = \hat{G}^{\alpha\alpha}\big[g(\boldsymbol{\zeta}), f(\boldsymbol{\zeta})\big], \tag{59e}$$

$$\hat{G}^{\alpha\alpha}\big[f_1(\zeta_1)g_1(\zeta_r), f_2(\zeta_1)g_2(\zeta_r)\big] = \hat{G}^{\alpha\alpha}\big[f_1(\zeta_1)g_2(\zeta_r), f_2(\zeta_1)g_1(\zeta_r)\big], \tag{59f}$$

where f, g, etc. are arbitrary functions of the independent variables specified in the equations, and the independent variables of $\hat{G}^{\beta\alpha}$ and $\hat{\nu}$ in equations (59a)–(59d) are shown in the respective last parentheses. Equations (59a) and (59b) follow from (17) and (18), and equations (59c) and (59d) follow from (33) and (38). Equations (59e) and (59f) are essentially the same as the corresponding relation for a single-component gas, the derivation of which is given in Ohwada [8].

It follows from equations (58a), (59a), and (59b) that

$$\Omega^{\beta\alpha jk}_{pqab} = \Omega^{\beta\alpha 0k}_{p-j,q-j,a,b}, \qquad \Lambda^{\beta\alpha jk}_{pa} = \Lambda^{\beta\alpha 0k}_{p-j,a}, \tag{60}$$

from (58b), (59c), and (59d) that

$$\Omega^{\beta\alpha 0k}_{pqab} = \Omega^{\beta\alpha 0k}_{-p,-q,a,b}, \qquad \Lambda^{\beta\alpha 0k}_{pa} = \Lambda^{\beta\alpha 0k}_{-p,a}, \tag{61}$$

and from (59e) and (59f) that

$$\Omega^{\alpha\alpha 0k}_{pqab} = \Omega^{\alpha\alpha 0k}_{qpba} = \Omega^{\alpha\alpha 0k}_{pqba}. \tag{62}$$

Equations (60) and (61) reduce the number of independent elements of $\Omega^{\beta\alpha jk}_{pqab}$ from $\mathrm{O}(N^6)$ to $\mathrm{O}(N^5)$ and that of $\Lambda^{\beta\alpha jk}_{pa}$ from $\mathrm{O}(N^4)$ to $\mathrm{O}(N^3)$, where N is the representative number of the lattice points of each molecular velocity component [i.e., N is of the order of $N_m + N_p + 1$ and of H].

4.3.2. Numerical kernels

From equations (33), (51a), and (57a), we obtain the following expression of $\Omega^{\beta\alpha 0k}_{pqab}$:

$$\begin{aligned}\Omega^{\beta\alpha 0k}_{pqab} = {}& \frac{\sqrt{2}}{\pi}\int_0^{\pi}\int_0^{\pi}\int_0^{\infty}\int_{-\infty}^{\infty}\int_{-\infty}^{\infty} \widetilde{\Psi}_p(J_1)\widetilde{\Psi}_q(K_1)\big(\sqrt{\hat{m}^{\beta}}J_r^{(k)}\big)^{2a}\big(\sqrt{\hat{m}^{\alpha}}K_r^{(k)}\big)^{2b} \\ & \times \exp\left(-\frac{(\sqrt{\hat{m}^{\beta}}J_r^{(k)})^2 + (\sqrt{\hat{m}^{\alpha}}K_r^{(k)})^2}{2}\right) z\sin\theta\,\mathrm{d}w'\,\mathrm{d}w''\,\mathrm{d}z\,\mathrm{d}\bar{\epsilon}\,\mathrm{d}\theta,\end{aligned} \tag{63}$$

where

$$J_1 = w''\sin\theta + (1-\hat{\mu}^{\beta\alpha}/\hat{m}^{\beta})z\cos\theta, \tag{64a}$$

$$J_r^{(k)} = \big\{\big(w' - \zeta_r^{\alpha(k)}\sin\bar{\epsilon}\big)^2 + \big[w''\cos\theta - \zeta_r^{\alpha(k)}\cos\bar{\epsilon} - (1-\hat{\mu}^{\beta\alpha}/\hat{m}^{\beta})z\sin\theta\big]^2\big\}^{1/2}, \tag{64b}$$

$$K_1 = (\hat{\mu}^{\beta\alpha}/\hat{m}^{\alpha})z\cos\theta, \tag{64c}$$

$$K_r^{(k)} = \big\{\big[(\hat{\mu}^{\beta\alpha}/\hat{m}^{\alpha})z\sin\theta + \zeta_r^{\alpha(k)}\cos\bar{\epsilon}\big]^2 + \big(\zeta_r^{\alpha(k)}\sin\bar{\epsilon}\big)^2\big\}^{1/2}. \tag{64d}$$

Because of the property (61), we only need $\Omega^{\beta\alpha 0k}_{pqab}$ for $q > 0$ and for $q = 0$, $p \geqslant 0$. For these p and q, equation (63) can be rewritten in the following form:

$$\Omega^{\beta\alpha 0k}_{pqab} = \frac{\sqrt{2}}{\pi}\int_0^{\pi/2}\int_0^{\pi} \Gamma^k_{pqab}(\theta,\bar{\epsilon})\,\mathrm{d}\bar{\epsilon}\,\mathrm{d}\theta \quad (q>0), \tag{65a}$$

$$\Omega^{\beta\alpha 0k}_{p0ab} = \frac{\sqrt{2}}{\pi}\int_0^{\pi/2}\int_0^{\pi} \left[\Gamma^k_{p0ab}(\theta,\bar{\epsilon}) + \Gamma^k_{-p,0,a,b}(\theta,\bar{\epsilon})\right]\mathrm{d}\bar{\epsilon}\,\mathrm{d}\theta \quad (p\geqslant 0), \tag{65b}$$

where

$$\Gamma^k_{pqab}(\theta,\bar{\epsilon}) = \sin\theta\int_0^{\infty} z\,\widetilde{\Psi}_q(K_1)\left(\sqrt{\hat{m}^\alpha}K_r^{(k)}\right)^{2b}\exp\left(-\frac{(\sqrt{\hat{m}^\alpha}K_r^{(k)})^2}{2}\right)\Theta^k_{pa}(z,\theta,\bar{\epsilon})\,\mathrm{d}z, \tag{66a}$$

$$\Theta^k_{pa}(z,\theta,\bar{\epsilon}) = \int_{-\infty}^{\infty}\int_{-\infty}^{\infty}\widetilde{\Psi}_p(J_1)\left(\sqrt{\hat{m}^\beta}J_r^{(k)}\right)^{2a}\exp\left(-\frac{(\sqrt{\hat{m}^\beta}J_r^{(k)})^2}{2}\right)\mathrm{d}w'\,\mathrm{d}w''. \tag{66b}$$

In equation (65a) we have omitted the part $[\pi/2,\ \pi]$ of the integration with respect to θ because $\widetilde{\Psi}_q$ is identically zero for the negative argument when $q>0$. In (65b), we have reduced the integral with respect to θ in (63) to that over $[0,\ \pi/2]$. This can be done by splitting the integral into that over $[0,\ \pi/2]$ and that over $[\pi/2,\ \pi]$, changing the variables as $w''=-w''$ and $\theta=\pi-\theta$ in the latter, and taking into account the property $\widetilde{\Psi}_p(-\zeta_1)=\widetilde{\Psi}_{-p}(\zeta_1)$. As shown in appendix B, equation (66b) can be integrated analytically. Therefore, the final expression of $\Omega^{\beta\alpha 0k}_{pqab}$ contains a triple integral with respect to z, $\bar{\epsilon}$, and θ. It is computed numerically by the Gauss–Legendre formula (Ralston and Rabinowitz [35]). (In the actual computation, we carry out the numerical integration using slightly different variables, i.e., $\bar{z}$, $\bar{\epsilon}$, and θ, as shown in appendix C.) When $\alpha=\beta$, Θ^k_{pa} does not depend on z (appendix B), and thus the integration with respect to z in equation (66a) can be performed analytically (see appendix C). Hence, the final expression of $\Omega^{\alpha\alpha 0k}_{pqab}$ contains double integral with respect to $\bar{\epsilon}$ and θ, which is computed numerically by the Gauss–Legendre formula. In the case of a single-component gas, the numerical kernel for the gain term is essentially the same as $\Omega^{\alpha\alpha 0k}_{pqab}$ (Ohwada [8]). Therefore, only the double integral (with respect to $\bar{\epsilon}$ and θ) should be calculated numerically to generate the numerical kernel. In the case of a binary mixture, one more integration (with respect to z) should be carried out numerically.

On the other hand, the integration with respect to $\bar{\phi}$ in equation (38) can be carried out and leads to the following expression for $\hat{\nu}[L]$:

$$\begin{aligned}\hat{\nu}[L] = 2\sqrt{2}\int_{-\infty}^{\infty}\int_0^{\infty}\left[(\zeta_{*1}-\zeta_1)^2+(\zeta_{*r}+\zeta_r)^2\right]^{1/2}\mathcal{E}_{II}\left(\frac{4\zeta_{*r}\zeta_r}{(\zeta_{*1}-\zeta_1)^2+(\zeta_{*r}+\zeta_r)^2}\right)\\ \times\zeta_{*r}L(\zeta_{*1},\zeta_{*r})\,\mathrm{d}\zeta_{*r}\,\mathrm{d}\zeta_{*1},\end{aligned} \tag{67}$$

where $\mathcal{E}_{II}$ is the complete elliptic integral of the second kind, i.e.,

$$\mathcal{E}_{II}(x) = \int_0^{\pi/2}\left(1-x\sin^2 t\right)^{1/2}\mathrm{d}t \quad (0\leqslant x\leqslant 1). \tag{68}$$

From equations (51b), (57a), and (67), the numerical kernel $\Lambda^{\beta\alpha 0k}_{pa}$ is expressed by

$$\begin{aligned}\Lambda^{\beta\alpha 0k}_{pa} = 2\sqrt{2}\int_{-\infty}^{\infty}\int_0^{\infty}\left[\zeta_{*1}^2+\left(\zeta_{*r}+\zeta_r^{\alpha(k)}\right)^2\right]^{1/2}\mathcal{E}_{II}\left(\frac{4\zeta_{*r}\zeta_r^{\alpha(k)}}{\zeta_{*1}^2+(\zeta_{*r}+\zeta_r^{\alpha(k)})^2}\right)\\ \times\zeta_{*r}\left(\hat{m}^\beta\zeta_{*r}^2\right)^a\exp\left(-\frac{\hat{m}^\beta\zeta_{*r}^2}{2}\right)\widetilde{\Psi}_p(\zeta_{*1})\,\mathrm{d}\zeta_{*r}\,\mathrm{d}\zeta_{*1}.\end{aligned} \tag{69}$$

The two-fold integration with respect to ζ_{*1} and ζ_{*r} in $\Lambda^{\beta\alpha 0k}_{pa}$ is carried out numerically by the Gauss–Legendre formula.

5. Results of numerical analysis

In this section, we show the results of numerical analysis, choosing the point at which $n(X_1) = (n_- + n_+)/2$ to be the origin $X_1 = 0$ of the X_1 coordinate.

5.1. Macroscopic quantities

To show the profiles of the molecular number densities n^α and n, the flow velocities (in the X_1 direction) v_1^α and v_1, and the temperatures T^α and T, we introduce the following quantities:

$$\tilde{n}^\alpha(X_1) = \frac{n^\alpha - n_-^\alpha}{n_+^\alpha - n_-^\alpha}, \qquad \tilde{n}(X_1) = \frac{n - n_-}{n_+ - n_-}, \tag{70a}$$

$$\tilde{v}_1^\alpha(X_1) = \frac{v_1^\alpha - U_+}{U_- - U_+}, \qquad \tilde{v}_1(X_1) = \frac{v_1 - U_+}{U_- - U_+}, \tag{70b}$$

$$\tilde{T}^\alpha(X_1) = \frac{T^\alpha - T_-}{T_+ - T_-}, \qquad \tilde{T}(X_1) = \frac{T - T_-}{T_+ - T_-}, \tag{70c}$$

where $\alpha = A, B$. The distributions of these variables are shown in *figures 1–4*: *figure 1* is for $M_- = 1.5$, $m^B/m^A = 0.5$, and $d_m^B/d_m^A = 1$; *figure 2* for $M_- = 3$, $m^B/m^A = 0.5$, and $d_m^B/d_m^A = 1$; *figure 3* for $M_- = 1.5$, $m^B/m^A = 0.25$, and $d_m^B/d_m^A = 1$; and *figure 4* for $M_- = 2$, $m^B/m^A = 0.25$, and $d_m^B/d_m^A = 1$. The downstream values n_+^α, U_+, T_+, and M_+ are given in the respective captions. The values of $n(X_1)$, $v_1(X_1)$, and $T(X_1)$ of the total mixture, which are obtained from the values at the lattice points by interpolation, are also shown in *tables I* and *II* for the cases corresponding to *figures 2* and *4*. The macroscopic variables of the light component (B-component) start to deviate from their upstream uniform values earlier than the corresponding variables of the heavy component (A-component). Then, the number density n^B and flow velocity v_1^B of the light component reach their downstream uniform values n_+^B and U_+ earlier. However, the temperature of the heavy component T^A rises more steeply and exceeds that of the light component T^B at a point inside the shock. Then, the former approaches the downstream equilibrium temperature monotonically or once becomes higher than the downstream temperature and then decreases to it (*figures 2*(*c*) and *4*(*c*)). These features appear more clearly when the mass ratio m^B/m^A is small (*figures 3* and *4*).

The aforementioned nonmonotonic distribution of the temperature T^A of the heavy component manifests itself when the concentration of the light component χ_-^B is large and the shock wave is not weak. This phenomenon has already been shown by the computations in the early stages (Beylich [25], Bird [29]) and has been known as the temperature overshoot (Bird [6,30]). As mentioned at the end of section 2.2, however, the following T_*^α, which is different from our T^α, is often adopted as the temperature of the individual components in the literature:

$$T_*^\alpha = \left(3kn^\alpha\right)^{-1} \int m^\alpha (\xi_i - v_1\delta_{i1})^2 F^\alpha \, \mathrm{d}\boldsymbol{\xi}. \tag{71}$$

The comparison of T_*^α with T^α is given in *figure 5*, where $\tilde{T}_*^\alpha$ is defined by

$$\tilde{T}_*^\alpha = \left(T_*^\alpha - T_-\right)/(T_+ - T_-). \tag{72}$$

As is seen from the figure, the overshoot is observed more clearly for T_*^A.

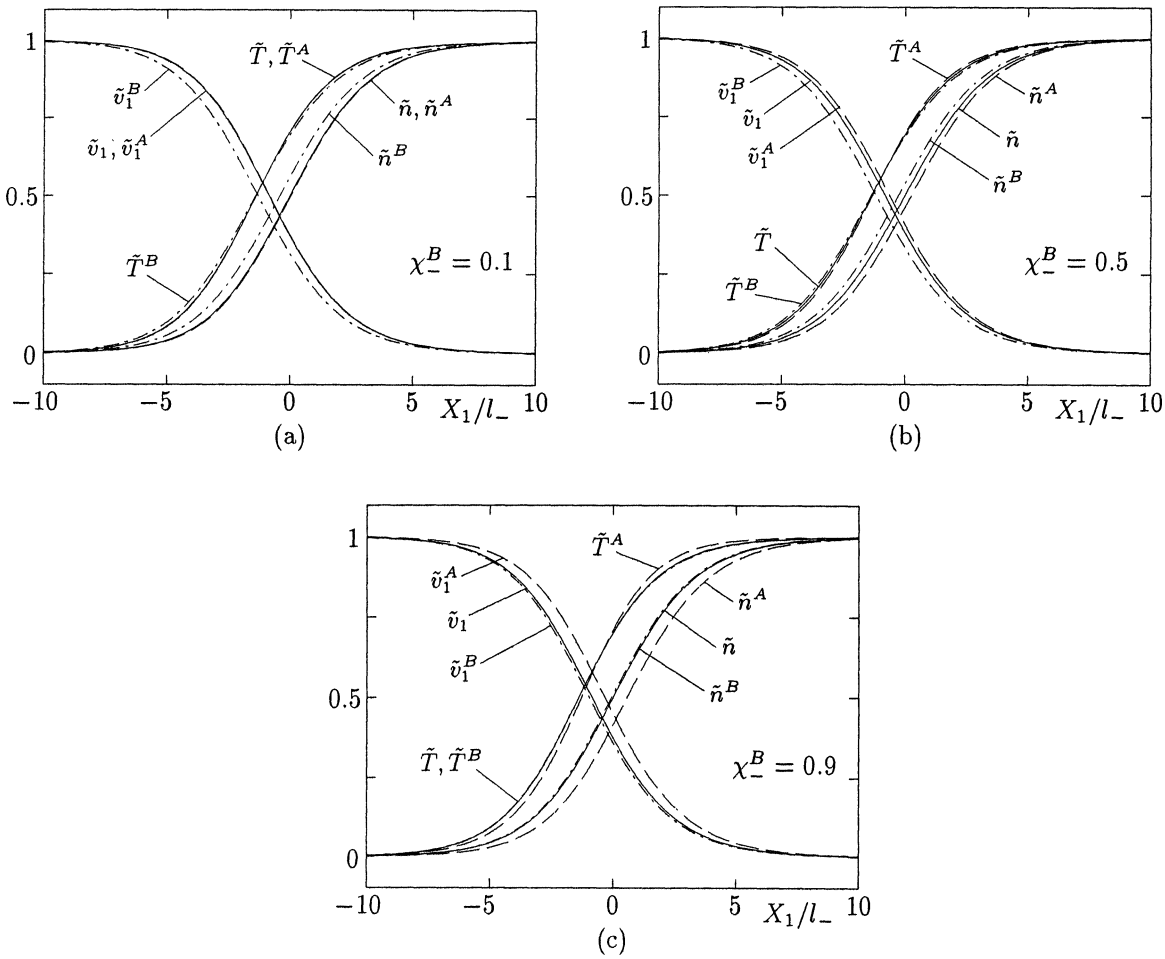

Figure 1. Profiles of molecular number densities, flow velocities, and temperatures for $M_- = 1.5$, $m^B/m^A = 0.5$, and $d_m^B/d_m^A = 1$: (a) $\chi_-^B = 0.1$, (b) $\chi_-^B = 0.5$, and (c) $\chi_-^B = 0.9$. For this M_-, the downstream values are $n_+^\alpha = 1.714 n_-^\alpha$, $U_+ = 0.5833 U_-$, $T_+ = 1.495 T_-$, and $M_+ = 0.7157$. Here, the solid lines indicate $\tilde{n}$, $\tilde{v}_1$, and $\tilde{T}$ for the total mixture, the dashed lines $\tilde{n}^A$, $\tilde{v}_1^A$, and $\tilde{T}^A$ for the A-component, and the dot–dash lines $\tilde{n}^B$, $\tilde{v}_1^B$, and $\tilde{T}^B$ for the B-component (see equation (70)).

5.2. Velocity distribution functions

Next we show the behavior of the velocity distribution functions. *Figures 6–9* show the nondimensional velocity distribution functions $\hat{F}^\alpha(x_1, \zeta_1, \zeta_r)$ $[= (2kT_-/m^A)^{3/2} n_-^{-1} F^\alpha(X_1, \xi_1, \xi_r);\ \xi_r = (\xi_2^2 + \xi_3^2)^{1/2}]$ ($\alpha = A, B$) as functions of ζ_1 $[= (2kT_-/m^A)^{-1/2}\xi_1]$ and ζ_r $[= (2kT_-/m^A)^{-1/2}\xi_r]$ at several points in the gas for $\chi_-^B = 0.5$ and $d_m^B/d_m^A = 1$; *figures 6* and *7* are for $M_- = 3$ and $m^B/m^A = 0.5$, and *figures 8* and *9* are for $M_- = 2$ and $m^B/m^A = 0.25$. Here, in consistency with the figures and tables in section 5.1, the positions in the gas are indicated by using the dimensional coordinate X_1. The equilibrium distributions at upstream infinity and those at downstream infinity are also shown in the figures. Compared with the upstream Maxwellians, the downstream Maxwellians, the centers of which are shifted (from U_- to U_+ in the dimensional ξ_i space), have lower heights and larger extents because of the increase of the temperature at downstream infinity. The figures clearly demonstrate the transition of the velocity distribution functions from the upstream to the downstream Maxwellians. In *figures 6* and *7*, corresponding to the peaks of the upstream and downstream Maxwellians, two

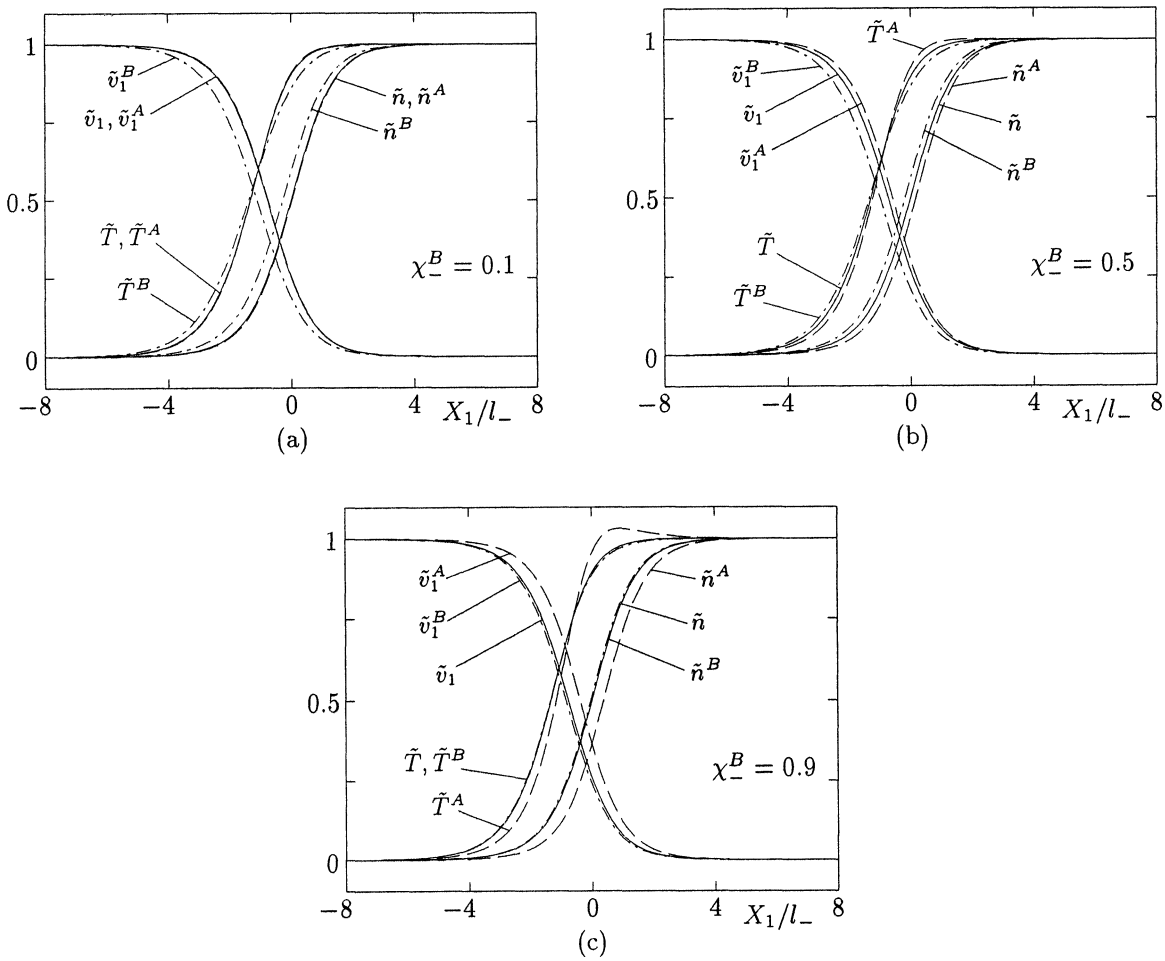

Figure 2. Profiles of molecular number densities, flow velocities, and temperatures for $M_- = 3$, $m^B/m^A = 0.5$, and $d_m^B/d_m^A = 1$: (a) $\chi_-^B = 0.1$, (b) $\chi_-^B = 0.5$, and (c) $\chi_-^B = 0.9$. For this M_-, the downstream values are $n_+^\alpha = 3n_-^\alpha$, $U_+ = U_-/3$, $T_+ = 3.667T_-$, and $M_+ = 0.5222$. See the caption of *figure 1*.

small lumps are observed both in $\hat{F}^A$ and $\hat{F}^B$ in the transition region (*figures 6*(*c*)–*6*(*e*) and *7*(*c*)–*7*(*e*)). As is seen from equations (21) and (22) and from *figures 6–9*, smaller mass ratio m^B/m^A makes the height of $\hat{F}^B$ lower and its extent larger for a fixed χ_-^B.

In *figures 10–13*, we show $\hat{F}^A$ and $\hat{F}^B$ at $\zeta_r = 0.15$ as functions of ζ_1 for several points in the gas. *Figures 10–13* correspond to the cases of *figures 1–4*, respectively, but the results for $\chi_-^B = 0.95$ are also included in the former figures.

5.3. Comparison with the DSMC computation

We have also carried out the computation of the problem by means of the standard DSMC method by Bird [6] for hard-sphere molecules in several cases. We here give some comparisons of the DSMC result with our present computation. *Figure 14* shows the profiles of the macroscopic variables corresponding to *figures 2*(*b*) and *4*(*b*), i.e., $M_- = 3$, $\chi_-^B = 0.5$, $m^B/m^A = 0.5$, and $d_m^B/d_m^A = 1$ (*figure 14*(*a*)), and $M_- = 2$, $\chi_-^B = 0.5$, $m^B/m^A = 0.25$, and $d_m^B/d_m^A = 1$ (*figure 14*(*b*)). In the figures, the DSMC results are shown by the symbols •, ○, and △, whereas

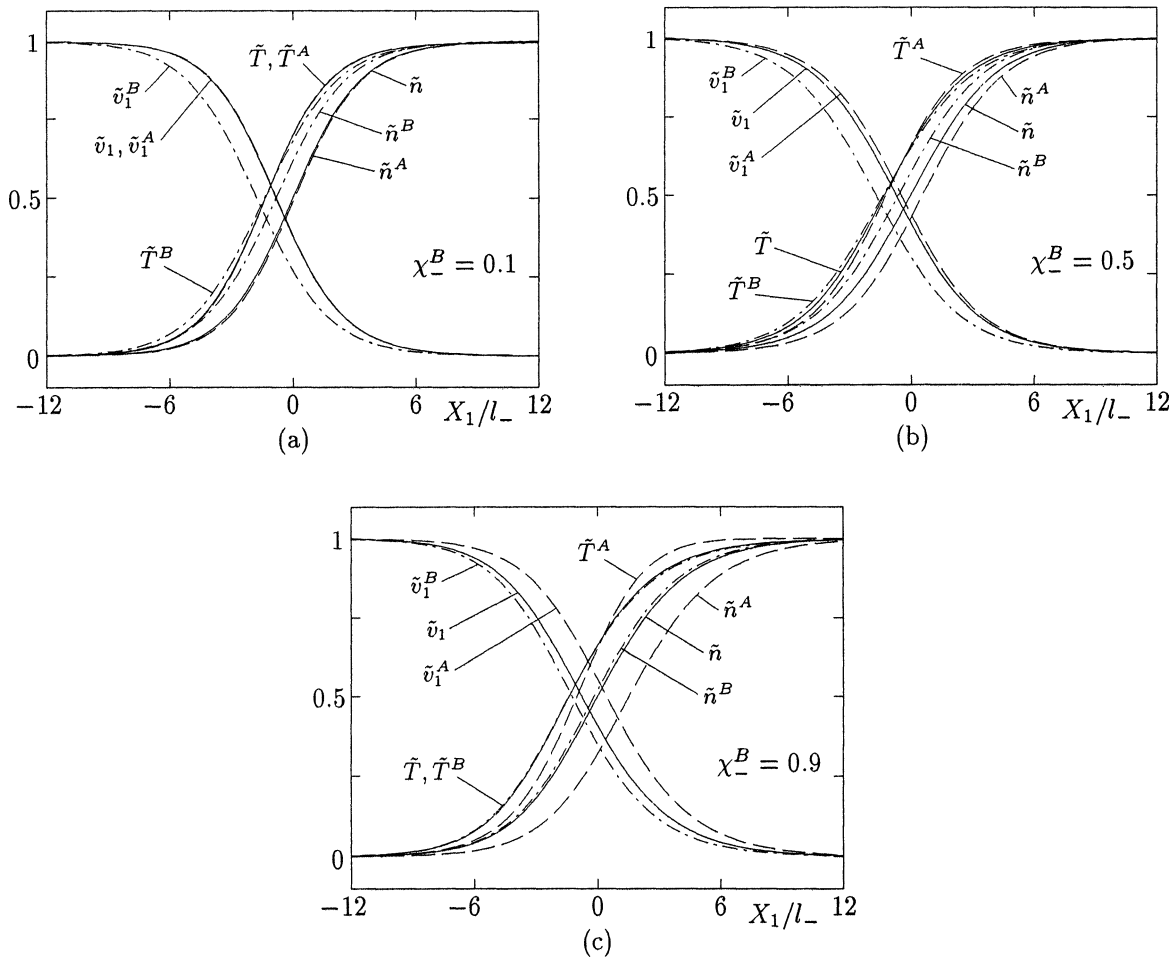

Figure 3. Profiles of molecular number densities, flow velocities, and temperatures for $M_- = 1.5$, $m^B/m^A = 0.25$, and $d_m^B/d_m^A = 1$: (a) $\chi_-^B = 0.1$, (b) $\chi_-^B = 0.5$, and (c) $\chi_-^B = 0.9$. For this M_-, the downstream values are $n_+^\alpha = 1.714 n_-^\alpha$, $U_+ = 0.5833 U_-$, $T_+ = 1.495 T_-$, and $M_+ = 0.7157$. See the caption of *figure 1*.

the results of our present computation by the solid, dashed, and dot-dash lines as in *figures 1–4*. On the other hand, *figure 15* shows the comparison of the velocity distribution function for the case of *figure 14*(*a*). To be more specific, the dimensionless velocity distribution functions $\hat{F}^A$ and $\hat{F}^B$ at $\zeta_r = 0.15$ and 1.35 are shown as the functions of ζ_1 for three points in the gas. The DSMC results show good agreement with those of the present computation for the velocity distribution function as well as for the macroscopic variables. The data about the present DSMC computation are as follows: 400 cells of a uniform size with length of $0.1 l_-$ are used, and the average number of simulation particles per cell is about 250 for each component in *figure 14*(*a*) and about 200 for each component in *figure 14*(*b*); the time step is $0.01 t_-$, where $t_- = l_-(2kT_-/m^A)^{-1/2}$; after the steady state has been established, the time average of 10 000 samples with sampling interval $0.5 t_-$ is taken, and the average is shown in *figures 14* and *15*. The short vertical bar above the profiles in *figure 14* indicates the standard deviation of the 10 000 samples for $\tilde{n}$ at the corresponding point, and that below the profiles indicate the larger value of the standard deviation for $\tilde{n}^A$ and that for $\tilde{n}^B$.

Table I. The distributions of the molecular number density n, flow velocity v_1, and temperature T of the total mixture for $M_- = 3$, $m^B/m^A = 0.5$, and $d_m^B/d_m^A = 1$ (cf. *figure 2*).

	n/n_-			$v_1/(2kT_-/m^A)^{1/2}$			T/T_-		
X_1/l_-	$\chi_-^B = 0.1$	$\chi_-^B = 0.5$	$\chi_-^B = 0.9$	$\chi_-^B = 0.1$	$\chi_-^B = 0.5$	$\chi_-^B = 0.9$	$\chi_-^B = 0.1$	$\chi_-^B = 0.5$	$\chi_-^B = 0.9$
$-\infty$	1.000	1.000	1.000	2.810	3.162	3.693	1.000	1.000	1.000
−6	1.001	1.001	1.001	2.807	3.158	3.688	1.008	1.009	1.009
−5	1.004	1.004	1.004	2.800	3.150	3.679	1.027	1.028	1.028
−4	1.012	1.013	1.013	2.778	3.125	3.649	1.084	1.087	1.088
−3	1.039	1.042	1.040	2.708	3.048	3.556	1.261	1.262	1.269
−2	1.127	1.134	1.131	2.501	2.821	3.281	1.748	1.732	1.758
−1.5	1.229	1.238	1.234	2.298	2.599	3.016	2.168	2.135	2.174
−1	1.400	1.409	1.406	2.019	2.294	2.654	2.659	2.607	2.656
−0.5	1.662	1.669	1.667	1.700	1.941	2.243	3.101	3.040	3.088
0	2.000	2.000	2.000	1.412	1.614	1.869	3.397	3.342	3.380
0.5	2.344	2.338	2.338	1.203	1.373	1.595	3.552	3.511	3.536
1	2.617	2.610	2.609	1.076	1.223	1.425	3.621	3.595	3.610
1.5	2.794	2.788	2.786	1.007	1.140	1.331	3.650	3.634	3.643
2	2.893	2.890	2.888	0.972	1.097	1.282	3.662	3.652	3.657
3	2.973	2.972	2.971	0.945	1.065	1.244	3.667	3.664	3.665
4	2.993	2.993	2.992	0.939	1.057	1.234	3.667	3.666	3.666
5	2.998	2.998	2.998	0.937	1.055	1.232	3.666	3.666	3.666
∞	3.000	3.000	3.000	0.937	1.054	1.231	3.667	3.667	3.667

Table II. The distributions of the molecular number density n, flow velocity v_1, and temperature T of the total mixture for $M_- = 2$, $m^B/m^A = 0.25$, and $d_m^B/d_m^A = 1$ (cf. *figure 4*).

	n/n_-			$v_1/(2kT_-/m^A)^{1/2}$			T/T_-		
X_1/l_-	$\chi_-^B = 0.1$	$\chi_-^B = 0.5$	$\chi_-^B = 0.9$	$\chi_-^B = 0.1$	$\chi_-^B = 0.5$	$\chi_-^B = 0.9$	$\chi_-^B = 0.1$	$\chi_-^B = 0.5$	$\chi_-^B = 0.9$
$-\infty$	1.000	1.000	1.000	1.898	2.309	3.203	1.000	1.000	1.000
−8	1.001	1.002	1.001	1.897	2.306	3.200	1.001	1.004	1.002
−6	1.004	1.010	1.006	1.892	2.293	3.187	1.010	1.021	1.014
−4	1.026	1.050	1.037	1.857	2.232	3.107	1.065	1.098	1.087
−3	1.065	1.105	1.088	1.794	2.148	2.984	1.159	1.198	1.195
−2	1.157	1.211	1.195	1.658	1.992	2.749	1.347	1.366	1.381
−1.5	1.238	1.291	1.280	1.552	1.882	2.587	1.479	1.474	1.496
−1	1.348	1.392	1.386	1.426	1.753	2.404	1.620	1.588	1.613
−0.5	1.486	1.511	1.510	1.292	1.614	2.218	1.752	1.700	1.720
0	1.643	1.643	1.643	1.167	1.478	2.042	1.860	1.798	1.811
0.5	1.799	1.776	1.773	1.063	1.357	1.889	1.938	1.878	1.882
1	1.938	1.899	1.890	0.985	1.258	1.764	1.991	1.940	1.937
2	2.129	2.088	2.068	0.894	1.127	1.592	2.046	2.015	2.006
3	2.222	2.194	2.174	0.855	1.062	1.498	2.066	2.050	2.042
4	2.261	2.246	2.230	0.840	1.033	1.449	2.073	2.065	2.060
6	2.283	2.279	2.273	0.832	1.014	1.413	2.077	2.075	2.073
8	2.286	2.285	2.283	0.831	1.011	1.404	2.077	2.077	2.076
∞	2.286	2.286	2.286	0.831	1.010	1.401	2.078	2.078	2.078

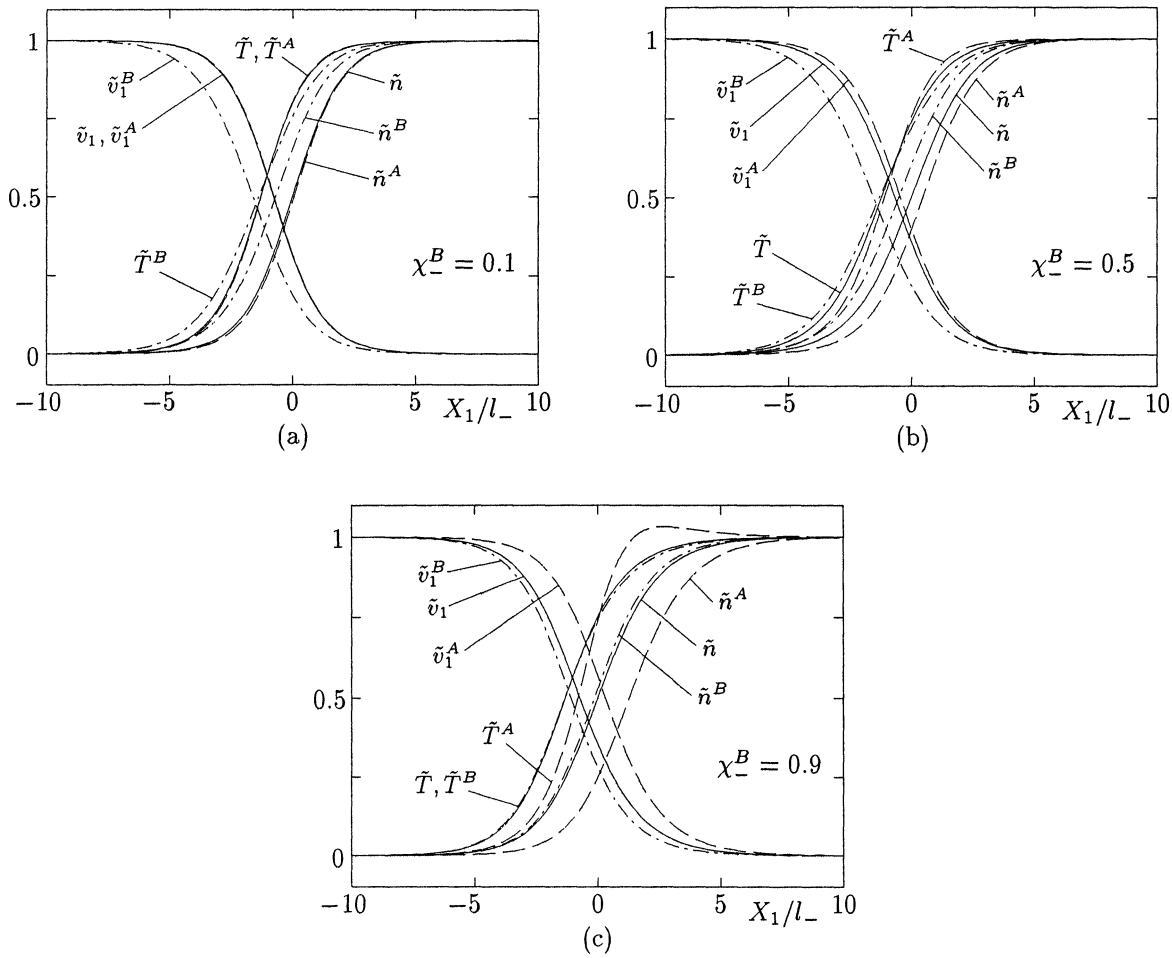

Figure 4. Profiles of molecular number densities, flow velocities, and temperatures for $M_- = 2$, $m^B/m^A = 0.25$, and $d_m^B/d_m^A = 1$: (a) $\chi_-^B = 0.1$, (b) $\chi_-^B = 0.5$, and (c) $\chi_-^B = 0.9$. For this M_-, the downstream values are $n_+^\alpha = 2.286 n_-^\alpha$, $U_+ = 0.4375 U_-$, $T_+ = 2.078 T_-$, and $M_+ = 0.6070$. See the caption of *figure 1*.

6. Data for computation and its accuracy

In this section, we use the original X_1 (or x_1) coordinate system, not the rearranged system used in section 5, unless the contrary is stated.

6.1. Lattice systems

We first summarize the lattice systems that are used in the actual computation. For the molecular velocity space, the four lattice systems ($\overline{\text{M1}}$), ($\overline{\text{M2}}$), (M3), and (M4) given in *table III* are used (see equations (52) and (55)). The reason why the bar is put on M1 and M2 is that, in ($\overline{\text{M1}}$) and ($\overline{\text{M2}}$) systems, ζ_r-lattice points slightly different from those explained in section 4.2 (cf. equation (52)) are used. That is, we assume the form

$$\hat{F}_i^{\alpha(n)}(\zeta_1^{\alpha(j)}, \zeta_r) = \exp\left(-\frac{\zeta_r^2}{2}\right) \sum_{m=0}^{H-1} a_{ijm}^{\alpha(n)} L_m(\zeta_r^2), \tag{73}$$

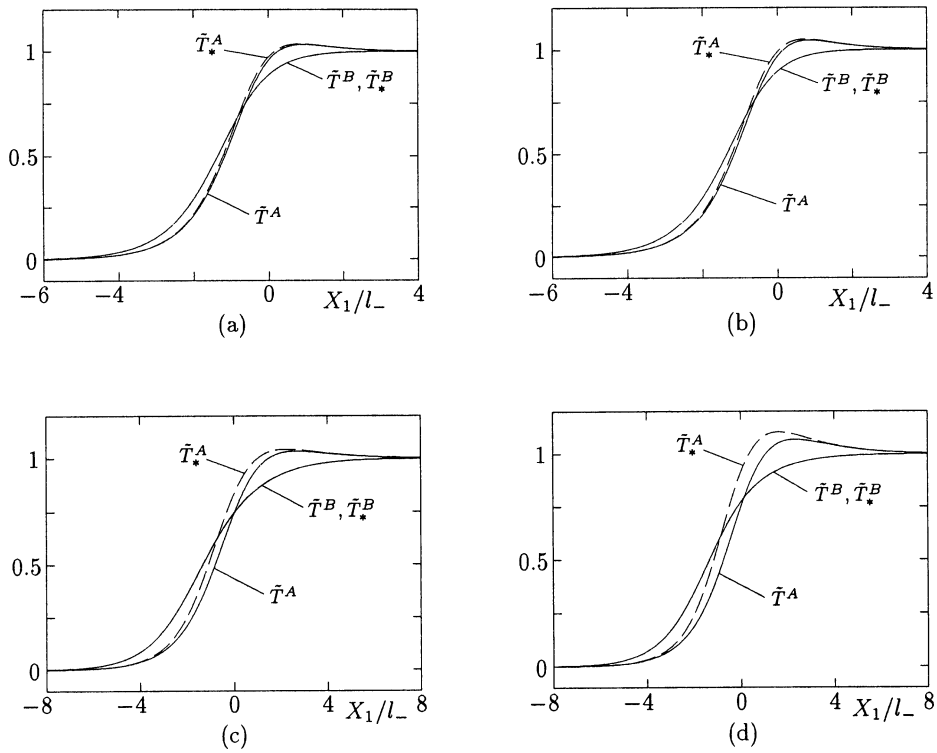

Figure 5. Profiles of T^α and T_*^α ($\alpha = A, B$) for $d_m^B/d_m^A = 1$: (a) $M_- = 3$, $m^B/m^A = 0.5$, $\chi_-^B = 0.9$, (b) $M_- = 3$, $m^B/m^A = 0.5$, $\chi_-^B = 0.95$, (c) $M_- = 2$, $m^B/m^A = 0.25$, $\chi_-^B = 0.9$, and (d) $M_- = 2$, $m^B/m^A = 0.25$, $\chi_-^B = 0.95$. Here, the solid line indicates $\tilde{T}^A$ and $\tilde{T}^B$ (see equation (70c)), and the dashed line $\tilde{T}_*^A$ and $\tilde{T}_*^B$ (see equation (72)).

Table III. Lattice systems in the molecular velocity space.

	N_m	N_p	h	H	$\zeta_1^{(-N_m)}$	$\zeta_1^{(N_p)}$	$\zeta_r^{\alpha(1)}$ or $\zeta_r^{(1)}$	$\zeta_r^{\alpha(H)}$ or $\zeta_r^{(H)}$
($\overline{\text{M1}}$)	26	34	0.25	14	−6.5	8.5	0.3158	6.6608
($\overline{\text{M2}}$)	44	56	0.15	14	−6.6	8.4	0.3158	6.6608
(M3)	60	73	0.15	14	−9.0	10.95	$0.3158/\sqrt{\hat{m}^\alpha}$	$6.6608/\sqrt{\hat{m}^\alpha}$
(M4)	66	81	0.15	14	−9.9	12.15	$0.3158/\sqrt{\hat{m}^\alpha}$	$6.6608/\sqrt{\hat{m}^\alpha}$
($\overline{\text{M5}}$)	44	56	0.15	18	−6.6	8.4	0.2796	7.6870
($\overline{\text{M6}}$)	60	73	0.15	18	−9.0	10.95	0.2796	7.6870
(M7)	44	56	0.15	14	−6.6	8.4	$0.3158/\sqrt{\hat{m}^\alpha}$	$6.6608/\sqrt{\hat{m}^\alpha}$
(M8)	60	73	0.15	14	−9.0	10.95	$0.3158/\sqrt{\hat{m}^\alpha}$	$6.6608/\sqrt{\hat{m}^\alpha}$

instead of equation (44) and use

$$\zeta_r^{\alpha(k)} = \zeta_r^{(k)} = \sqrt{y_k} \quad (k = 1, \ldots, H), \tag{74}$$

instead of equation (52). As a result, the forms of numerical kernels $\Omega_{pqab}^{\beta\alpha 0k}$ and $\Lambda_{pa}^{\beta\alpha 0k}$ undergo slight changes (in fact, $\Omega_{pqab}^{AA0k} = \Omega_{pqab}^{BB0k}$ holds and $\Lambda_{pa}^{\beta\alpha 0k}$ becomes independent of the labels α and β, which are the advantage of this choice). Since the changes are rather straightforward, we omit them here. This choice works when the molecular masses m^A and m^B are not very different ($0.5 \lesssim m^B/m^A$ when $m^B < m^A$). The edges of the domain

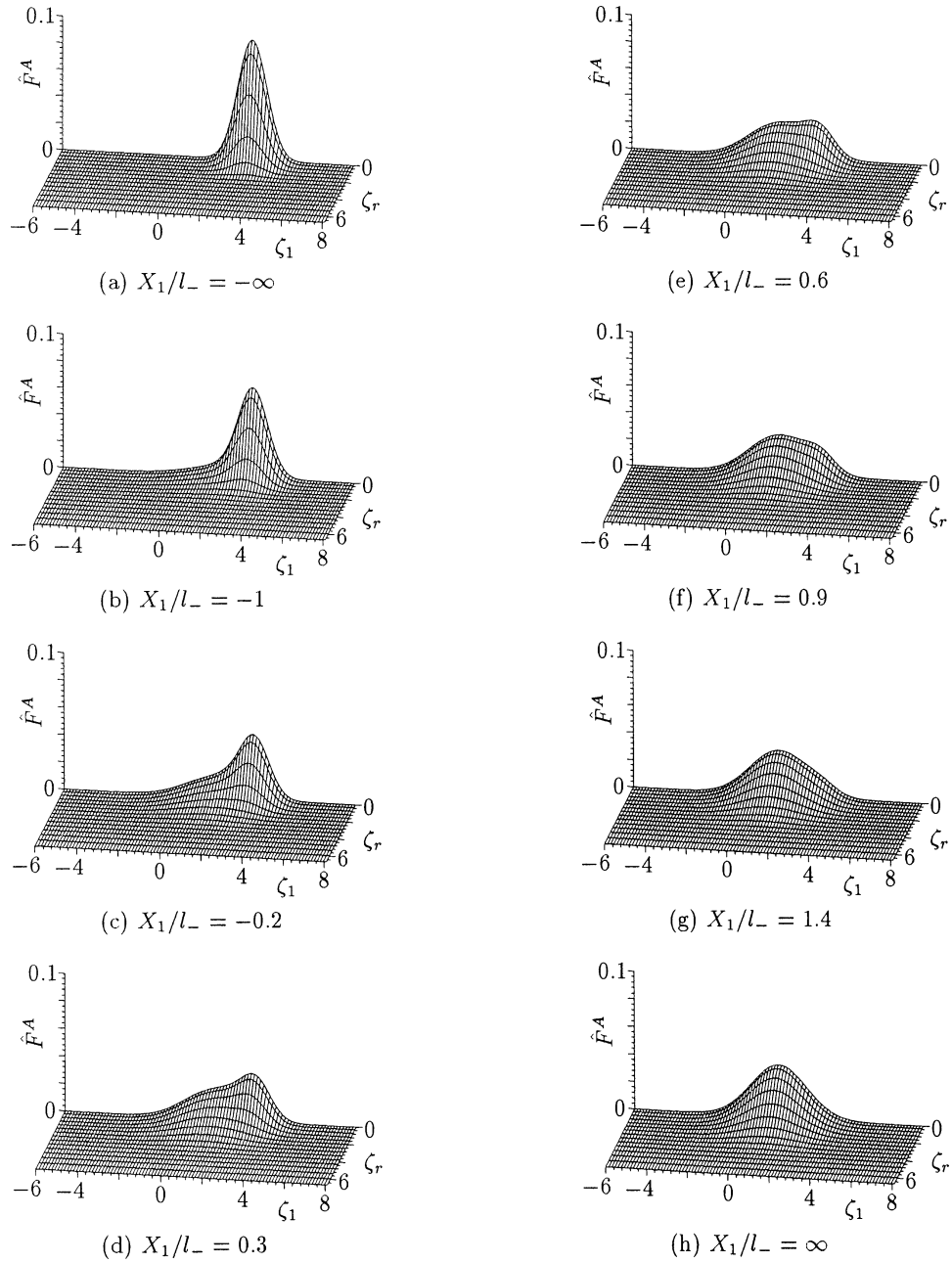

Figure 6. Dimensionless velocity distribution function $\hat{F}^A$ at eight points in the gas for $M_- = 3$, $\chi_-^B = 0.5$, $m^B/m^A = 0.5$, and $d_m^B/d_m^A = 1$ (cf. *figure 2*(*b*)): (a) $X_1/l_- = -\infty$, (b) $X_1/l_- = -1$, (c) $X_1/l_- = -0.2$, (d) $X_1/l_- = 0.3$, (e) $X_1/l_- = 0.6$, (f) $X_1/l_- = 0.9$, (g) $X_1/l_- = 1.4$, and (h) $X_1/l_- = \infty$.

in ζ_1, i.e., $\zeta_1^{(-N_m)}$ and $\zeta_1^{(N_p)}$, and the first and last lattice points in ζ_r, i.e., $\zeta_r^{\alpha(1)}$ and $\zeta_r^{\alpha(H)}$ (or $\zeta_r^{(1)}$ and $\zeta_r^{(H)}$), for the systems ($\overline{\text{M1}}$), ($\overline{\text{M2}}$), (M3), and (M4) are also shown in *table III*. The computer memory required for the numerical kernels corresponding to these four systems is: ($\overline{\text{M1}}$): 263MB, ($\overline{\text{M2}}$): 720MB, (M3): 1.4GB, and (M4): 1.7GB.

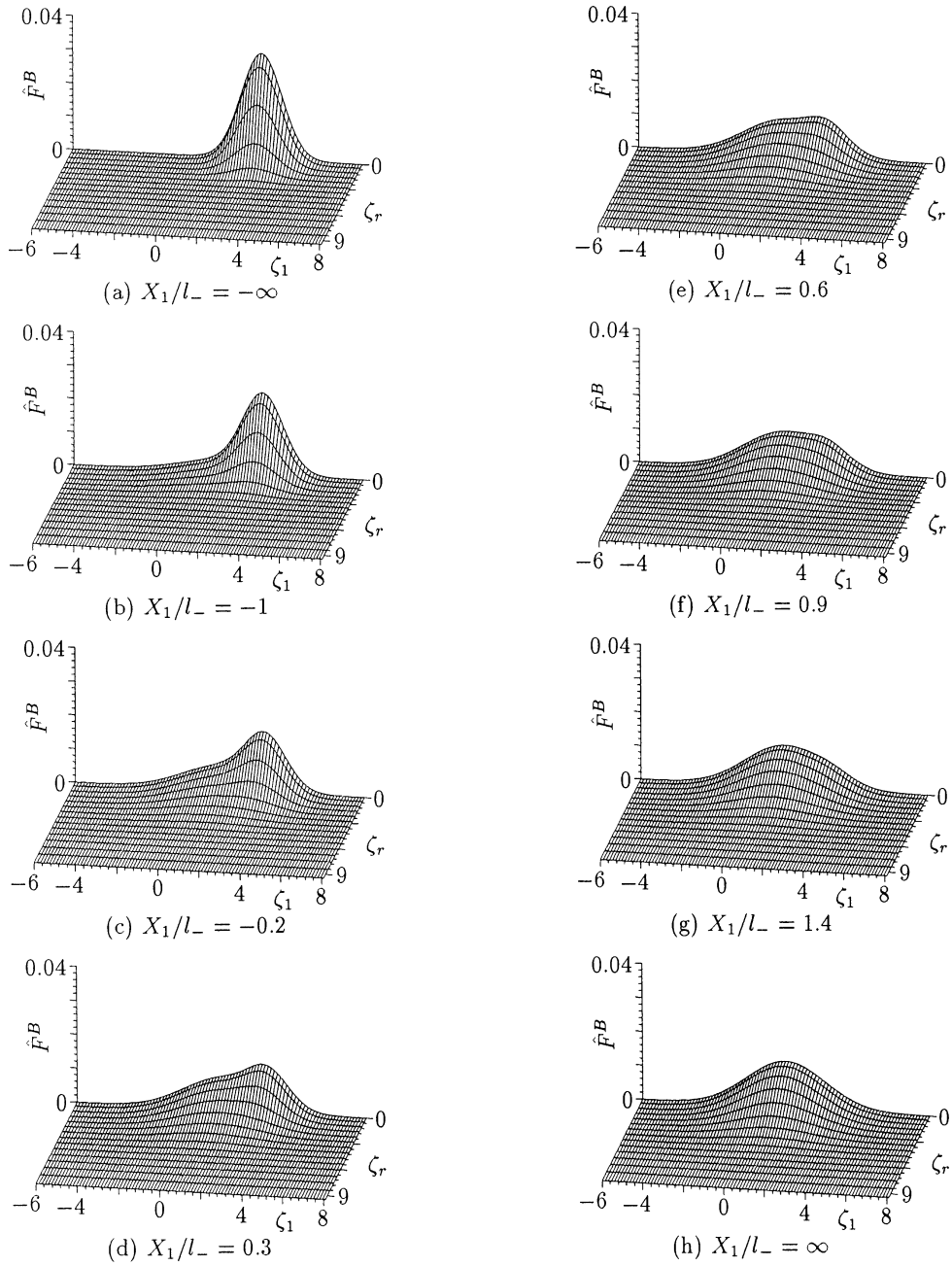

Figure 7. Dimensionless velocity distribution function $\hat{F}^B$ at eight points in the gas for $M_- = 3$, $\chi_-^B = 0.5$, $m^B/m^A = 0.5$, and $d_m^B/d_m^A = 1$ (cf. *figure 2*(*b*)): (a) $X_1/l_- = -\infty$, (b) $X_1/l_- = -1$, (c) $X_1/l_- = -0.2$, (d) $X_1/l_- = 0.3$, (e) $X_1/l_- = 0.6$, (f) $X_1/l_- = 0.9$, (g) $X_1/l_- = 1.4$, and (h) $X_1/l_- = \infty$.

The lattice system for the space coordinate x_1 is defined by

$$x_1^{(i)} = f_\delta \bar{x}_1^{(i)} \qquad (i = -N_D, \ldots, 0, \ldots, N_D), \tag{75}$$

where

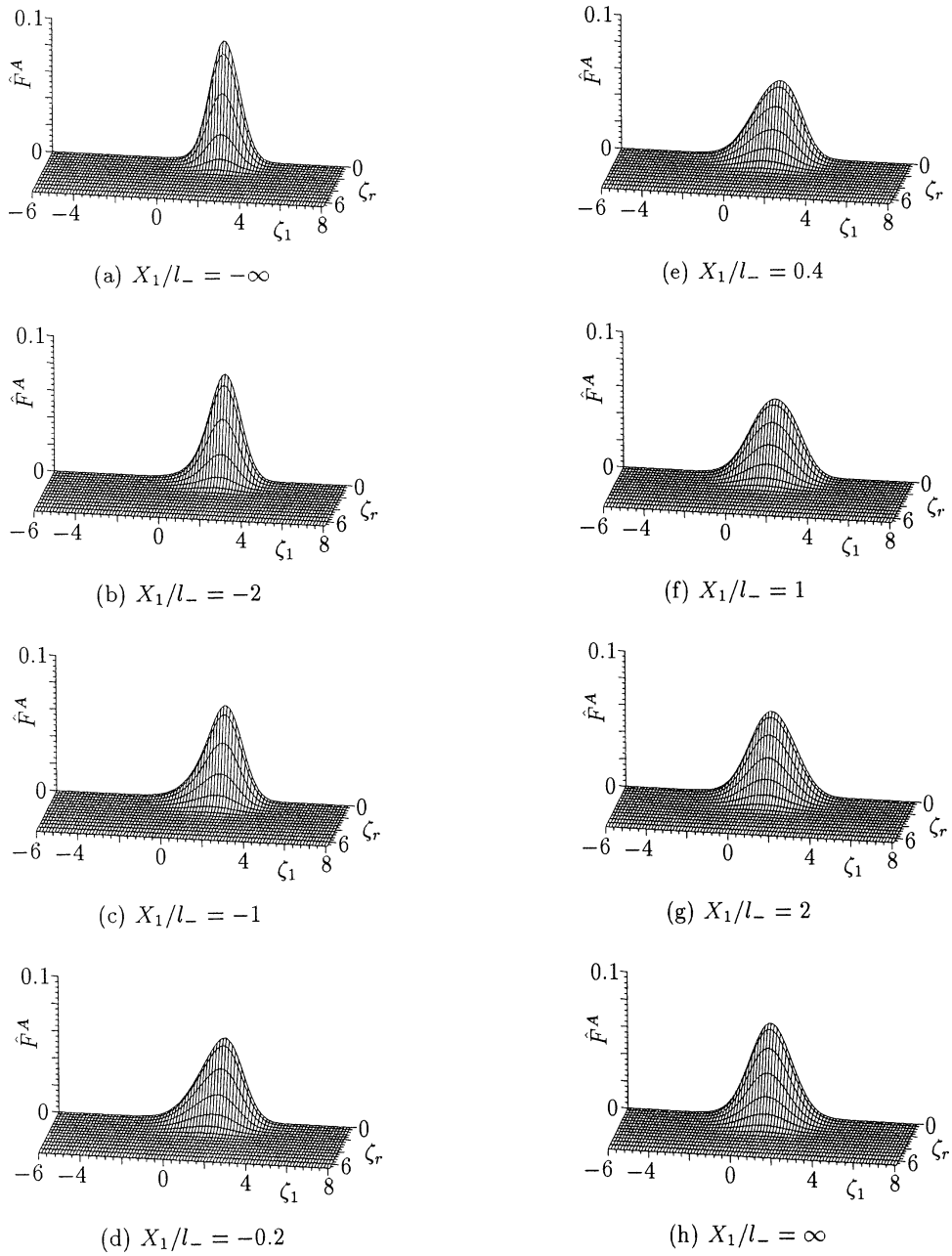

Figure 8. Dimensionless velocity distribution function $\hat{F}^A$ at eight points in the gas for $M_- = 2$, $\chi_-^B = 0.5$, $m^B/m^A = 0.25$, and $d_m^B/d_m^A = 1$ (cf. *figure 4(b)*): (a) $X_1/l_- = -\infty$, (b) $X_1/l_- = -2$, (c) $X_1/l_- = -1$, (d) $X_1/l_- = -0.2$, (e) $X_1/l_- = 0.4$, (f) $X_1/l_- = 1$, (g) $X_1/l_- = 2$, and (h) $X_1/l_- = \infty$.

$$f_\delta = \frac{\sqrt{\frac{m^B}{m^A}}\chi_-^A + \chi_-^B}{\sqrt{\frac{m^B}{m^A}}(\chi_-^A)^2 + 2\left(\frac{d_m^{BA}}{d_m^A}\right)^2\sqrt{\frac{m^B+m^A}{2m^A}}\chi_-^A\chi_-^B + \left(\frac{d_m^B}{d_m^A}\right)^2(\chi_-^B)^2}, \tag{76a}$$

$$\bar{x}_1^{(i)} = \frac{50d'}{N_D}i + \left[\operatorname{erf}(3.5) - \operatorname{erf}\left(3.5 \times \frac{N_D - i}{N_D}\right)\right](D' - 50d') \quad (i = 0, \ldots, N_D - 1), \tag{76b}$$

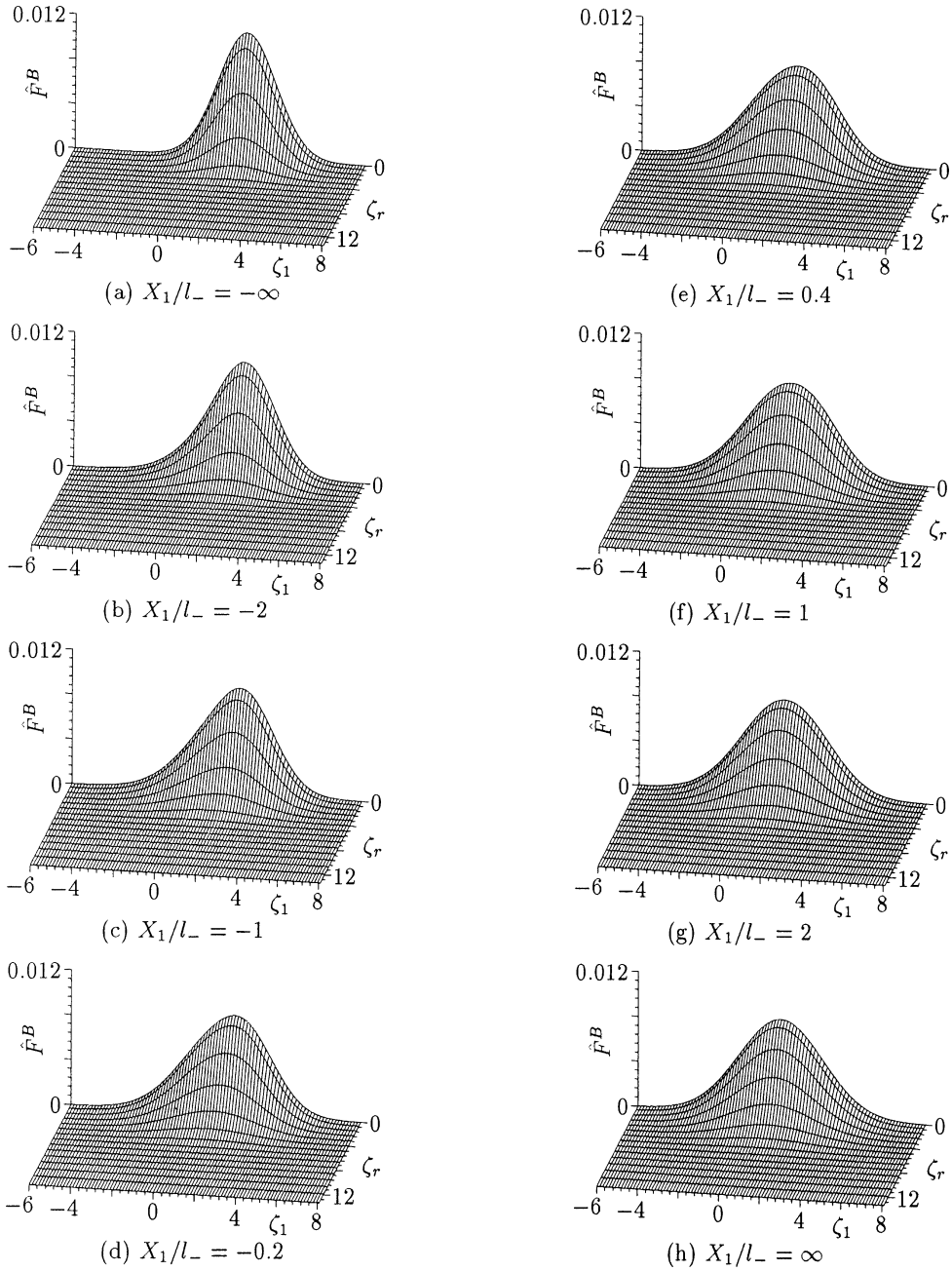

Figure 9. Dimensionless velocity distribution function $\hat{F}^B$ at eight points in the gas for $M_- = 2$, $\chi_-^B = 0.5$, $m^B/m^A = 0.25$, and $d_m^B/d_m^A = 1$ (cf. *figure 4*(*b*)): (a) $X_1/l_- = -\infty$, (b) $X_1/l_- = -2$, (c) $X_1/l_- = -1$, (d) $X_1/l_- = -0.2$, (e) $X_1/l_- = 0.4$, (f) $X_1/l_- = 1$, (g) $X_1/l_- = 2$, and (h) $X_1/l_- = \infty$.

$$\bar{x}_1^{(N_D)} = D', \tag{76c}$$

$$\bar{x}_1^{(-i)} = -\bar{x}_1^{(i)}, \tag{76d}$$

and $\mathrm{erf}(x)$ is the error function defined by (B11). Equation (75) means that the X_1 coordinate is rescaled by $f_\delta l_-$ and then the lattice points are set in the rescaled coordinate $X_1/f_\delta l_-$. This is because in the $X_1/f_\delta l_-$ coordinate,

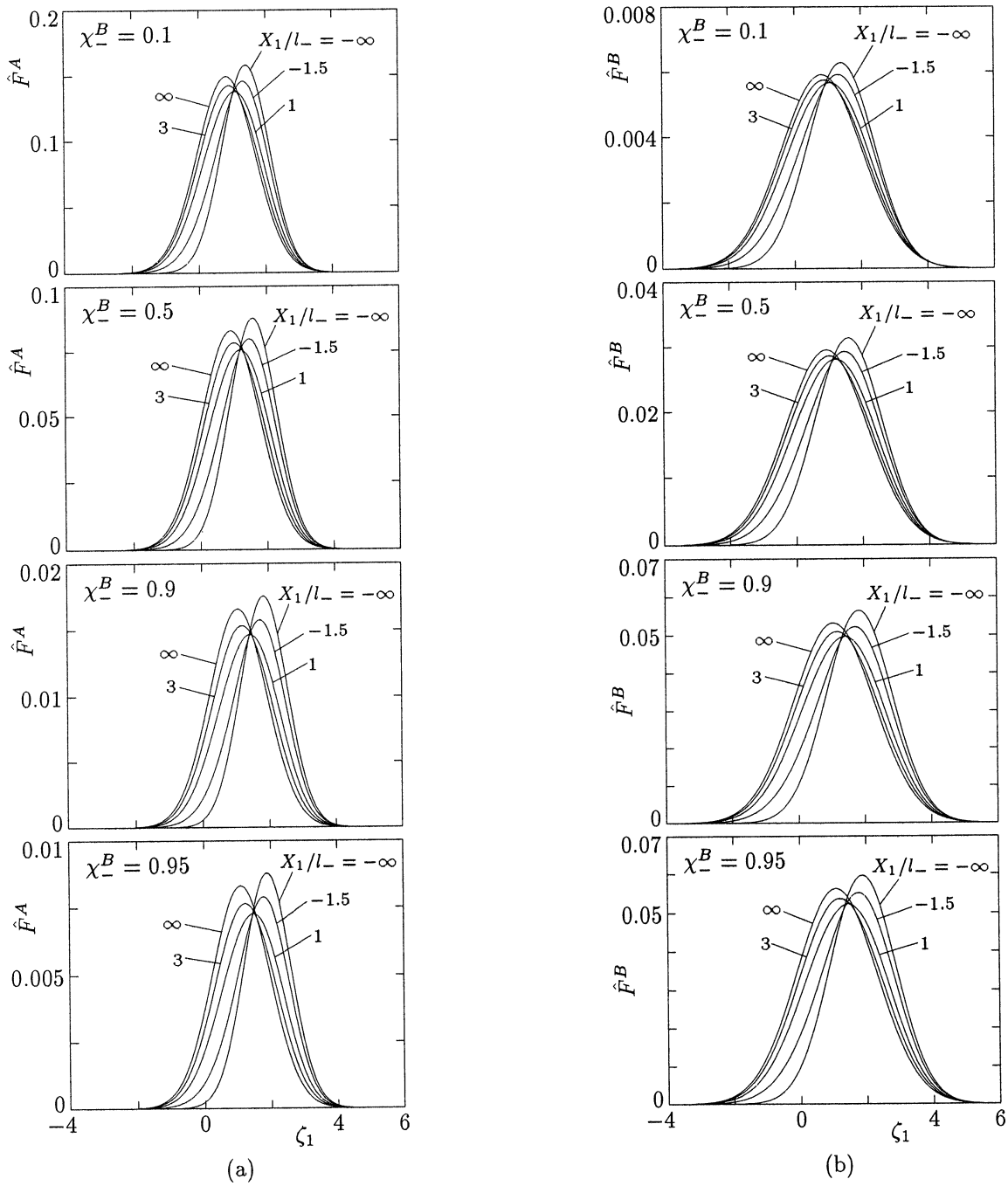

Figure 10. Dimensionless velocity distribution functions $\hat{F}^A$ and $\hat{F}^B$ at $\zeta_r = 0.15$ for $M_- = 1.5$, $m^B/m^A = 0.5$, and $d_m^B/d_m^A = 1$: (a) $\hat{F}^A$, (b) $\hat{F}^B$. The $\hat{F}^A$ and $\hat{F}^B$ at several points in the gas are shown for $\chi_-^B = 0.1$, $\chi_-^B = 0.5$, $\chi_-^B = 0.9$, and $\chi_-^B = 0.95$.

the shock thickness is less sensitive to the change in the parameters m^B/m^A, d_m^B/d_m^A, and χ_-^B than in the X_1/l_- (or x_1) coordinate. However, f_δ is almost unity ($0.973 < f_\delta < 1$) for the values of the parameters chosen in our computation. We use the following two systems for the computation:

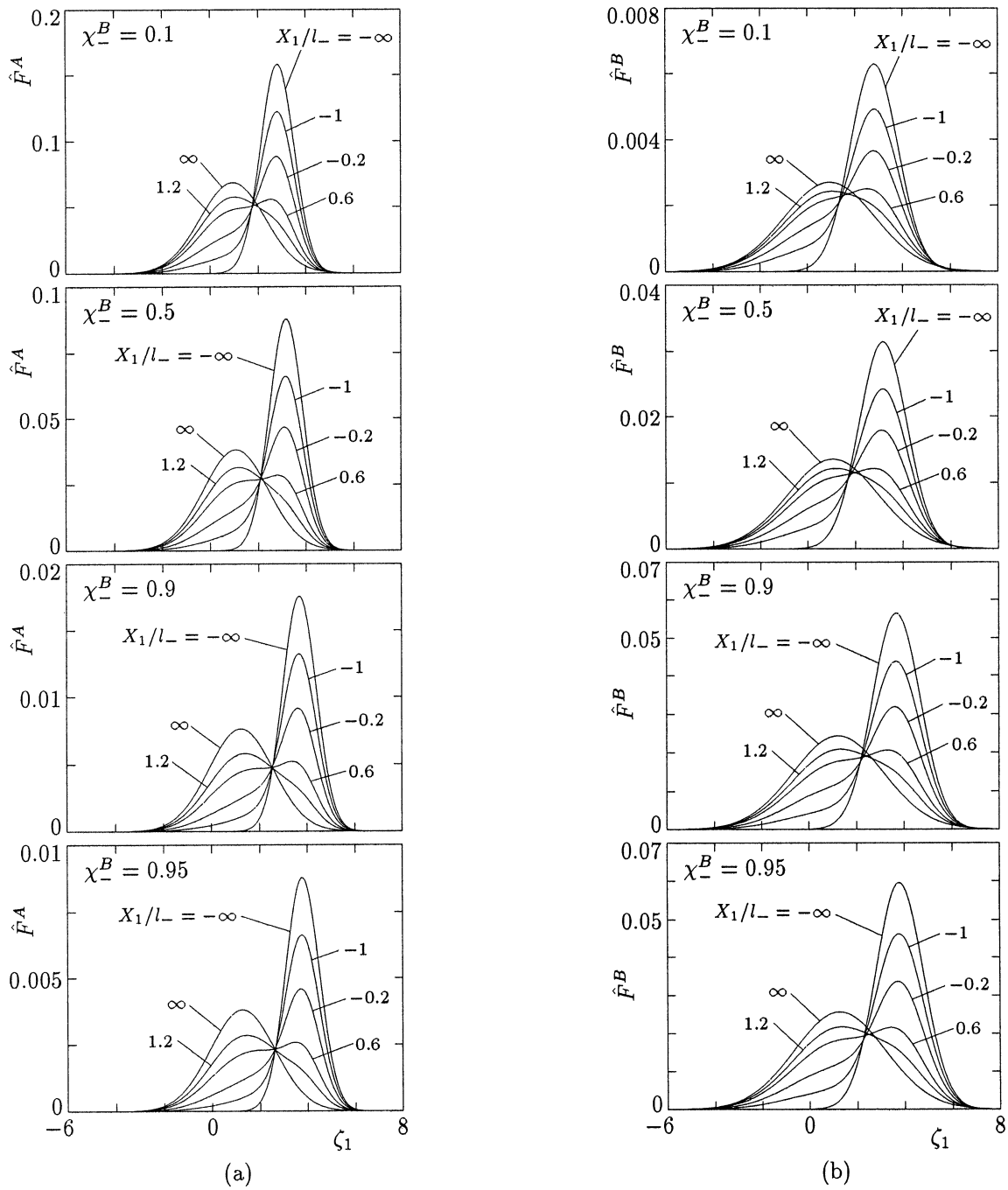

Figure 11. Dimensionless velocity distribution functions $\hat{F}^A$ and $\hat{F}^B$ at $\zeta_r = 0.15$ for $M_- = 3$, $m^B/m^A = 0.5$, and $d_m^B/d_m^A = 1$: (a) $\hat{F}^A$, (b) $\hat{F}^B$. See the caption of *figure 10*.

(S1): $D' = 10\sqrt{\pi}$ $(= 17.7245)$, $N_D = 25$, $d' = 0.05\sqrt{\pi}$ $(= 0.088623)$,
(S2): $D' = 10\sqrt{\pi}$, $N_D = 50$, $d' = 0.05\sqrt{\pi}$.

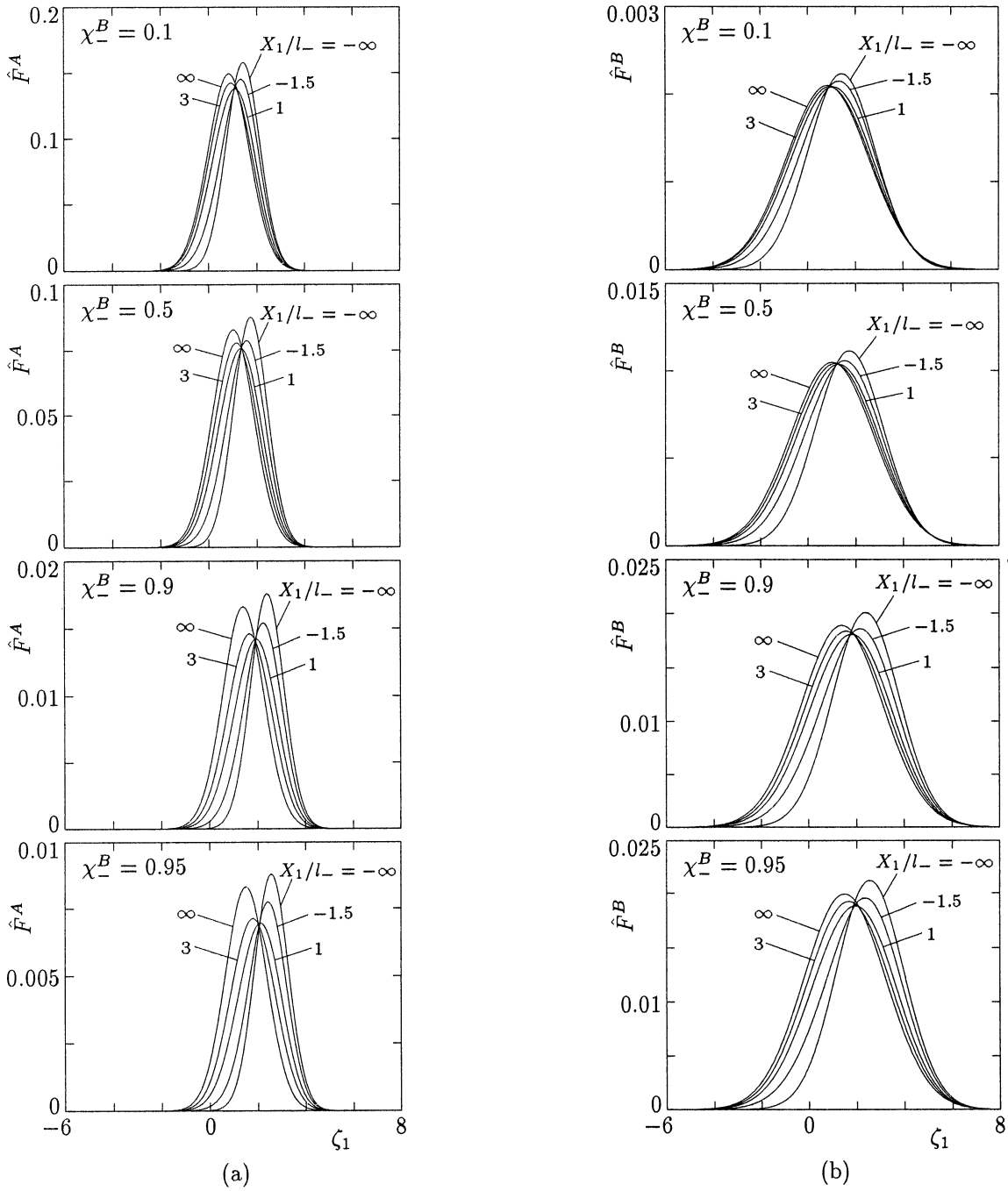

Figure 12. Dimensionless velocity distribution functions $\hat{F}^A$ and $\hat{F}^B$ at $\zeta_r = 0.15$ for $M_- = 1.5$, $m^B/m^A = 0.25$, and $d_m^B/d_m^A = 1$: (a) $\hat{F}^A$, (b) $\hat{F}^B$. See the caption of *figure 10*.

The lattice interval is minimum at $x_1 = 0$ ($x_1^{(1)} - x_1^{(0)} = 0.1773 f_\delta$ for (S1) and $0.08863 f_\delta$ for (S2)) and increases, with the increase of $|x_1|$, to the maximum value at the edge of the domain, $|x_1| = 17.7245 f_\delta$ ($x_1^{(N_D)} - x_1^{(N_D-1)} = 2.264 f_\delta$ for (S1) and $1.137 f_\delta$ for (S2)).

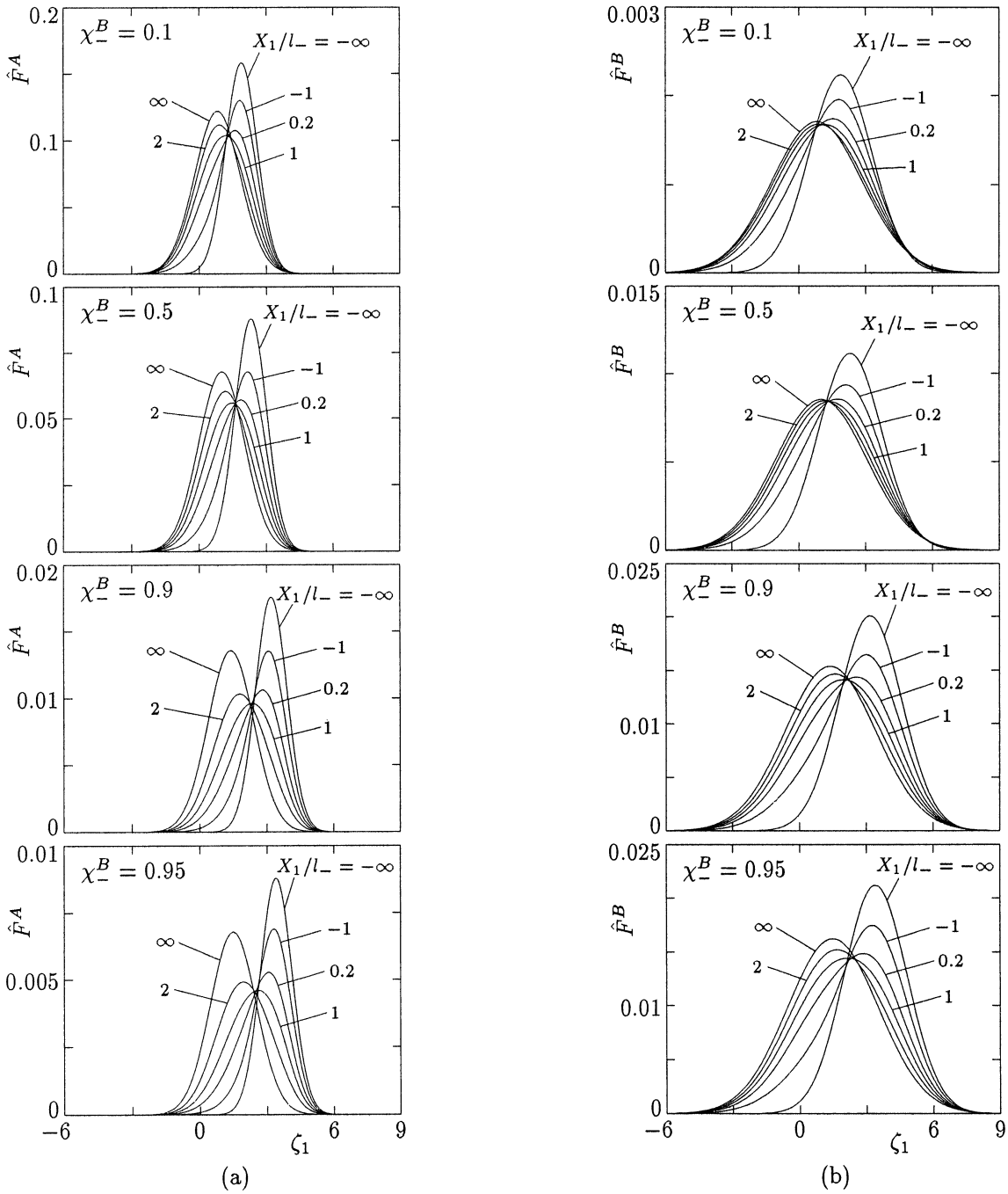

Figure 13. Dimensionless velocity distribution functions $\hat{F}^A$ and $\hat{F}^B$ at $\zeta_r = 0.15$ for $M_- = 2$, $m^B/m^A = 0.25$, and $d_m^B/d_m^A = 1$: (a) $\hat{F}^A$, (b) $\hat{F}^B$. See the caption of *figure 10*.

The data for ($M_- = 1.5$, $m^B/m^A = 0.5$) in section 5 are based on the ($\overline{\text{M2}}$; S2) system, those for ($M_- = 3$, $m^B/m^A = 0.5$) are based on the (M3; S2) system, and those for $m^B/m^A = 0.25$ are based on the (M4; S2) system. The ($\overline{\text{M1}}$) and (S1) systems are used for accuracy test. The computing time for one iteration (the steps

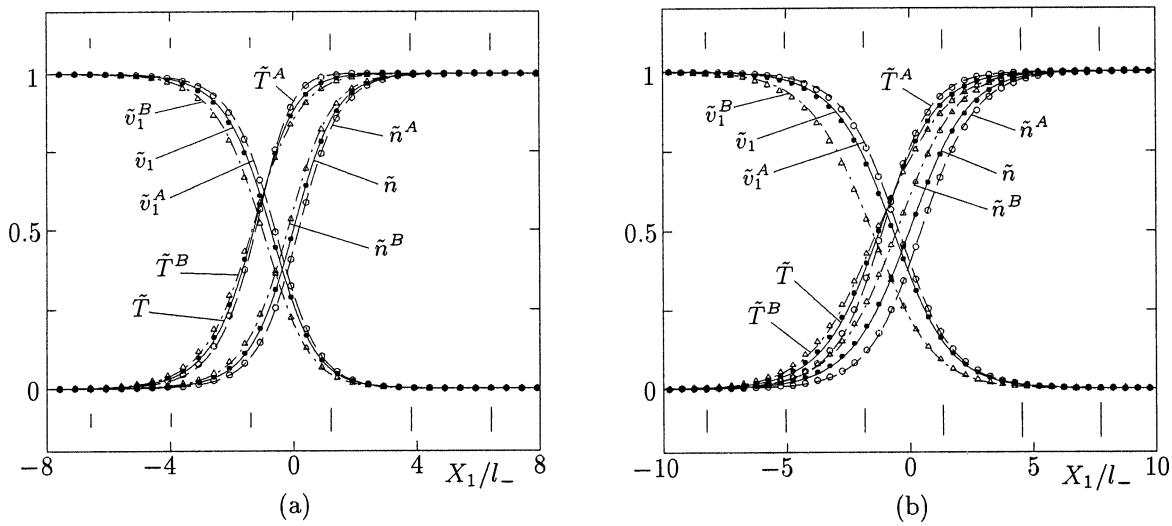

Figure 14. Comparison with the DSMC results; profiles of molecular number densities, flow velocities, and temperatures: (a) $M_- = 3$, $\chi_-^B = 0.5$, $m^B/m^A = 0.5$, and $d_m^B/d_m^A = 1$ (see *figure 2*(*b*)), (b) $M_- = 2$, $\chi_-^B = 0.5$, $m^B/m^A = 0.25$, and $d_m^B/d_m^A = 1$ (see *figure 4*(*b*)). The results obtained by the DSMC method are shown by the symbols • ($\tilde{n}$, $\tilde{v}_1$, and $\tilde{T}$), ○ ($\tilde{n}^A$, $\tilde{v}_1^A$, and $\tilde{T}^A$), and △ ($\tilde{n}^B$, $\tilde{v}_1^B$, and $\tilde{T}^B$). The results by the present finite-difference method are shown by the solid line ($\tilde{n}$, $\tilde{v}_1$, and $\tilde{T}$), dashed line ($\tilde{n}^A$, $\tilde{v}_1^A$, and $\tilde{T}^A$), and dot–dash line ($\tilde{n}^B$, $\tilde{v}_1^B$, and $\tilde{T}^B$). The short vertical bar above the profiles indicates the standard deviation of the samples for $\tilde{n}$ at the corresponding point, and that below the profiles the larger value of the standard deviation for $\tilde{n}^A$ and that for $\tilde{n}^B$.

(i)–(iv) in section 4.1) in a parallel computation using ten CPU's on a VPP800 computer (see the last paragraph of section 7) is as follows: 9 sec for ($\overline{\text{M1}}$; S2) system; 46 sec for ($\overline{\text{M2}}$; S2) system; 99 sec for (M3; S2) system; and 142 sec for (M4; S2) system.

6.2. Criterion for convergence

In order to save the number of iterations, we use the following initial distributions $\hat{F}_{ijk}^{\alpha(0)}$. For $\chi_-^B = 0.5$, we first compute the corresponding numerical solution of the model Boltzmann equation proposed by Garzó et al. [36] by a finite-difference method and use the solution as $\hat{F}_{ijk}^{\alpha(0)}$. Then we carry out the iteration process described in section 4.1 to obtain the desired solution for $\chi_-^B = 0.5$. For other values of χ_-^B, we use $\hat{F}_{ijk}^{\alpha(0)}$ obtained by suitable modification of the solution (of the Boltzmann equation) for $\chi_-^B = 0.5$.

In the actual computation, however, even after the profiles of the macroscopic variables seem to have converged, the profiles move by a small but almost constant value in each iteration. This is due to the fact that the Rankine–Hugoniot relation (1) is not satisfied exactly because of the computational error. Therefore, we set the following criterion for the convergence. Let us denote by $\hat{n}^{(m)}(x_1)$ the dimensionless number density $n(X_1)/n_-$ of the total mixture corresponding to the solution $\hat{F}_{ijk}^{\alpha(m)}$ at the mth step of iteration, and let us denote by S_m the x_1 coordinate at which $\hat{n}^{(m)}(x_1)$ takes the value $(1+n_+/n_-)/2$ (i.e., n(at mth iteration) $= (n_- + n_+)/2$ at $x_1 = S_m$). That is, $x_1 = S_m$ is the 'center' of the shock wave at the mth iteration. Now we introduce the shift of the center in 20 steps, i.e.,

$$(\Delta S)_{20l} = S_{20l} - S_{20(l-1)} \quad (l = 1, 2, \ldots). \tag{77}$$

Then, we examine the change of the profile of the number density relative to the center in the 20 steps, i.e., we introduce the following quantity:

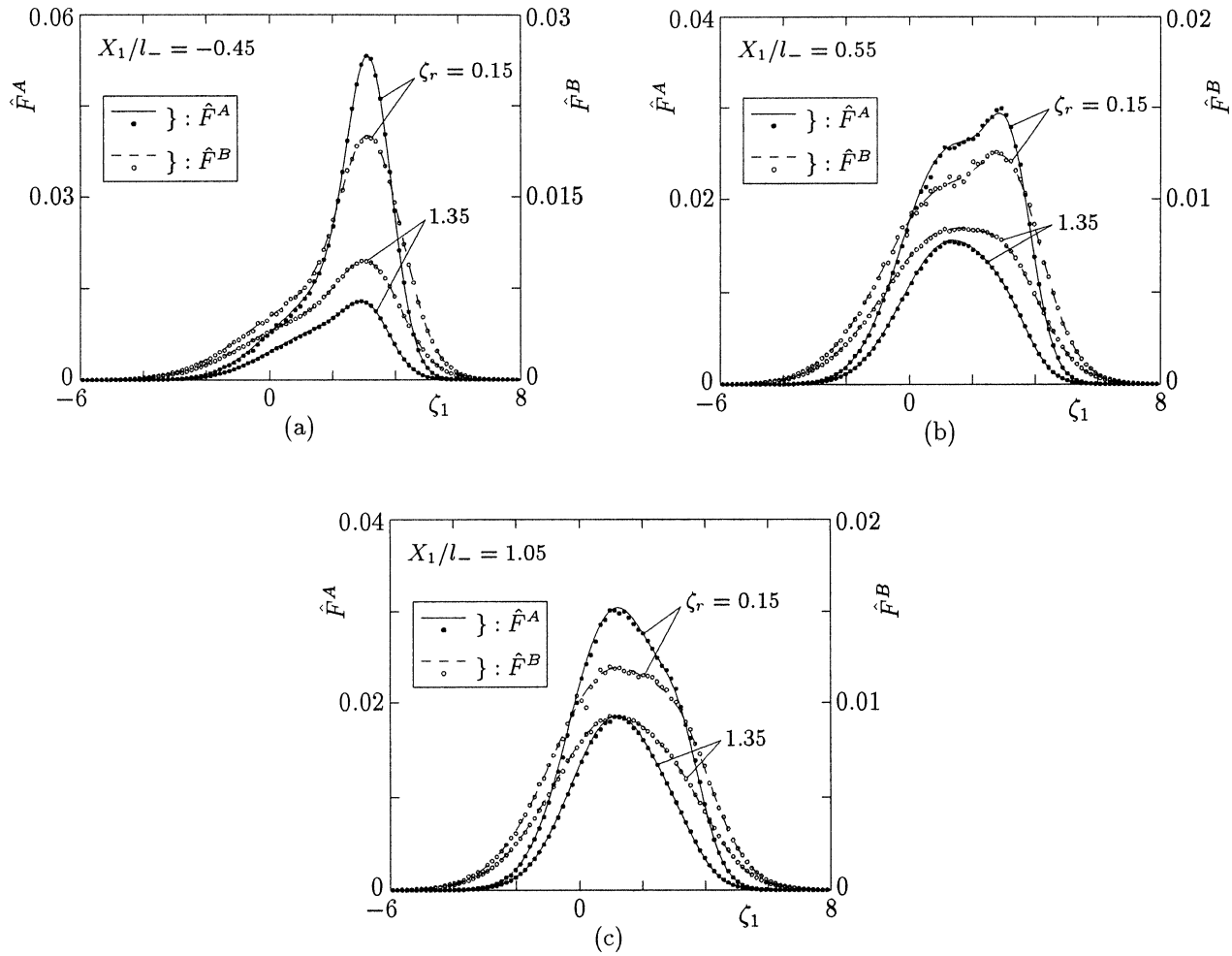

Figure 15. Comparison with the DSMC results; dimensionless velocity distribution functions $\hat{F}^A$ and $\hat{F}^B$ at $\zeta_r = 0.15$ and 1.35 for $M_- = 3$, $\chi_-^B = 0.5$, $m^B/m^A = 0.5$, and $d_m^B/d_m^A = 1$: (a) $X_1/l_- = -0.45$, (b) $X_1/l_- = 0.55$, (c) $X_1/l_- = 1.05$. The results obtained by the DSMC method are shown by • ($\hat{F}^A$) and ∘ ($\hat{F}^B$). The results by the present finite-difference method by solid line ($\hat{F}^A$) and dashed line ($\hat{F}^B$).

$$(\Delta\hat{n})_{20l} = \max_i \{ |\hat{n}^{(20l)}(x_1^{(i)} + (\Delta S)_{20l}) - \hat{n}^{(20(l-1))}(x_1^{(i)})| \text{ at } i = 0, \pm 5, \pm 10 \ldots \ (|i| < N_D) \}. \tag{78}$$

Here, the values $\hat{n}^{(20l)}(x_1^{(i)} + (\Delta S)_{20l})$ are computed by means of interpolation. When the condition $(\Delta\hat{n})_{20l} < 10^{-5}$ is satisfied, we stop the iteration judging that the solution has converged. Then, we regard the result of the last iteration as the desired steady solution. The necessary iteration steps n_*, the shift of the center $(\Delta S)_{n_*}$ in the final 20 steps, and the difference $|(\Delta S)_{n_*} - (\Delta S)_{n_*-20}|$ between the shift in the final 20 steps and that in the preceding 20 steps in the cases of *figures 1*(*b*), *2*(*b*), *3*(*b*), and *4*(*b*) are as follows:

$n_* = 280$, $(\Delta S)_{n_*} = 2.80 \times 10^{-3}$, $|(\Delta S)_{n_*} - (\Delta S)_{n_*-20}| = 4.83 \times 10^{-5}$ for *figure 1*(*b*);
$n_* = 320$, $(\Delta S)_{n_*} = 7.34 \times 10^{-4}$, $|(\Delta S)_{n_*} - (\Delta S)_{n_*-20}| = 1.90 \times 10^{-6}$ for *figure 2*(*b*);
$n_* = 360$, $(\Delta S)_{n_*} = 8.50 \times 10^{-3}$, $|(\Delta S)_{n_*} - (\Delta S)_{n_*-20}| = 7.36 \times 10^{-5}$ for *figure 3*(*b*);
$n_* = 480$, $(\Delta S)_{n_*} = 2.70 \times 10^{-3}$, $|(\Delta S)_{n_*} - (\Delta S)_{n_*-20}| = 1.45 \times 10^{-5}$ for *figure 4*(*b*).

The initial distributions $\hat{F}^{\alpha(0)}_{ijk}$ are arranged in such a way that the center of the shock at the final stage of iteration stays in the vicinity of the origin of the original coordinate system. As a result, if we denote by $x_1 = S_{n_*}$ the position of the center at the final stage, $|S_{n_*}|$ is less than 0.6 for all the cases in section 5.

6.3. Accuracy of computation

The accuracy of computation can be estimated by comparing the macroscopic quantities for the different lattice systems. Let $\sigma(\mathrm{M}, \mathrm{S})$ represent n, v_1, and T obtained by the use of lattice systems (M, S) (M= $\overline{\mathrm{M1}}$, $\overline{\mathrm{M2}}$, and M3, and S=S1 and S2). We introduce the maximum difference of the two results based on two different lattice systems (M, S) and (M′, S′) by

$$\mathsf{D}(\mathrm{M}', \mathrm{S}'; \mathrm{M}, \mathrm{S}) = \max_{\sigma=n, v_1, T} \left(\max_{X_1} \frac{|\sigma(\mathrm{M}', \mathrm{S}') - \sigma(\mathrm{M}, \mathrm{S})|}{\sigma(\mathrm{M}, \mathrm{S})} \right), \tag{79}$$

where $|\sigma(\mathrm{M}', \mathrm{S}') - \sigma(\mathrm{M}, \mathrm{S})|/\sigma(\mathrm{M}, \mathrm{S})$ is evaluated at about 2000 uniformly distributed points in the rearranged X_1 coordinate system (see the first sentence of section 5) by means of interpolation, and the maximum with respect to X_1 is taken over these points. The values of D for some test computations for $m^B/m^A = 0.5$, $d^B_m/d^A_m = 1$, and $M_- = 1.5$ or 2 are given as follows.

$$\mathsf{D}(\overline{\mathrm{M1}}, \mathrm{S2}; \overline{\mathrm{M2}}, \mathrm{S2}) = \begin{cases} 8.09 \times 10^{-4} & (M_- = 1.5,\ \chi^B_- = 0.95), \\ 1.97 \times 10^{-3} & (M_- = 2,\ \chi^B_- = 0.1), \\ 1.23 \times 10^{-3} & (M_- = 2,\ \chi^B_- = 0.5), \\ 6.57 \times 10^{-4} & (M_- = 2,\ \chi^B_- = 0.9), \\ 5.78 \times 10^{-4} & (M_- = 2,\ \chi^B_- = 0.95), \end{cases}$$

$$\mathsf{D}(\overline{\mathrm{M1}}, \mathrm{S2}; \mathrm{M3}, \mathrm{S2}) = 1.30 \times 10^{-3} \quad (M_- = 2,\ \chi^B_- = 0.5),$$

$$\mathsf{D}(\overline{\mathrm{M2}}, \mathrm{S2}; \mathrm{M3}, \mathrm{S2}) = 4.17 \times 10^{-4} \quad (M_- = 2,\ \chi^B_- = 0.5),$$

$$\mathsf{D}(\overline{\mathrm{M2}}, \mathrm{S1}; \overline{\mathrm{M2}}, \mathrm{S2}) = 1.46 \times 10^{-3} \quad (M_- = 2,\ \chi^B_- = 0.5).$$

Another measure of accuracy is given by the conservation laws. That is, by integrating equation (5) ($\alpha = A, B$), $\sum_{\alpha=A,B}[m^\alpha \xi_1 \times$ equation (5)], and $\sum_{\alpha=A,B}[m^\alpha \xi_j^2 \times$ equation (5)] over the whole space of ξ_i respectively and by taking into account the fact that the gas is in the equilibrium distribution (10) (for all ξ_1) at upstream infinity, we have

$$J^\alpha_M = \int \xi_1 F^\alpha \, \mathrm{d}\boldsymbol{\xi} = n^\alpha_- U_-, \tag{80a}$$

$$J_P = \int \sum_{\alpha=A,B} m^\alpha \xi_1^2 F^\alpha \, \mathrm{d}\boldsymbol{\xi} = k n_- T_- + \rho_- U_-^2, \tag{80b}$$

$$J_E = \frac{1}{2} \int \sum_{\alpha=A,B} m^\alpha \xi_1 \xi_j^2 F^\alpha \, \mathrm{d}\boldsymbol{\xi} = \frac{1}{2} U_- \left(5 k n_- T_- + \rho_- U_-^2\right), \tag{80c}$$

where $\rho_- = \sum_{\alpha=A,B} m^\alpha n^\alpha_-$. Here, J^α_M, J_P, and J_E are, respectively, the flux in the X_1 direction of the particle of the α-component, that of the X_1 component of the total momentum, and that of the total energy. The J^α_M, J_P, and J_E do not depend on X_1 theoretically. But, in the actual computation, the values of these fluxes deviate slightly from the RHS's of equation (80) and vary with X_1 because of the computational error. This deviation provides a measure of accuracy of the computation. Let us denote by $(J^\alpha_M)_c$, $(J_P)_c$, and $(J_E)_c$ the fluxes J^α_M, J_P,

and J_E obtained by the numerical computation and by $(J_M^\alpha)_e$, $(J_P)_e$, and $(J_E)_e$ their exact values (i.e., RHS's of equation (80)). Then, we introduce the following relative difference:

$$\mathsf{E} = \max_{J=J_M^\alpha, J_P, J_E} \Big(\max_{X_1} \big| \big[(J)_c - (J)_e \big] / (J)_e \big| \Big), \tag{81}$$

where the maximum with respect to X_1 is taken over the original lattice points. For the results shown in section 5, we give the estimate of E here. For $m^B/m^A = 0.5$ and $d_m^B/d_m^A = 1$ (cf. *figures 1, 2, 10*, and *11*),

$$\mathsf{E} \leqslant \begin{cases} 4.55 \times 10^{-4} & (M_- = 1.5,\ \chi_-^B = 0.1), \\ 1.77 \times 10^{-4} & (M_- = 1.5,\ \chi_-^B = 0.5,\ 0.9,\ 0.95), \\ 2.12 \times 10^{-4} & (M_- = 3,\ \chi_-^B = 0.1,\ 0.5), \\ 3.51 \times 10^{-4} & (M_- = 3,\ \chi_-^B = 0.9,\ 0.95), \end{cases}$$

and for $m^B/m^A = 0.25$ and $d_m^B/d_m^A = 1$ (cf. *figures 3, 4, 12*, and *13*),

$$\mathsf{E} \leqslant \begin{cases} 5.71 \times 10^{-4} & (M_- = 1.5,\ \chi_-^B = 0.1,\ 0.5), \\ 3.72 \times 10^{-4} & (M_- = 1.5,\ \chi_-^B = 0.9,\ 0.95), \\ 3.19 \times 10^{-4} & (M_- = 2,\ \chi_-^B = 0.1,\ 0.5,\ 0.9,\ 0.95). \end{cases}$$

Next, we give some information about the values of the velocity distribution functions at (or near) the edges of the range of computation in X_1 and ξ_1 for the results given in section 5. For convenience, we use the nondimensional form in the following discussions. Let $\hat{F}_-^\alpha(\zeta_1, \zeta_r)$ and $\hat{F}_+^\alpha(\zeta_1, \zeta_r)$ denote the upstream Maxwellian (equation (21) for all ζ_1) and the downstream one (equation (22) for all ζ_1), respectively. Then, the maxima of $\hat{F}_-^\alpha$ and $\hat{F}_+^\alpha$ are, respectively, $(\hat{F}_-^\alpha)_{\max} = \pi^{-3/2}(\hat{m}^\alpha)^{3/2}\chi_-^\alpha$ and $(\hat{F}_+^\alpha)_{\max} = \pi^{-3/2}(\hat{m}^\alpha)^{3/2}\chi_-^\alpha(n_+^\alpha/n_-^\alpha)(T_+/T_-)^{-3/2}$. At the edge of the computational range in ζ_1, i.e., at $\zeta_1 = \zeta_1^{(-N_m)}$ and $\zeta_1^{(N_p)}$ (cf. *table III*), the values of $\hat{F}^\alpha$ are

$$\hat{F}^A/(\hat{F}_-^A)_{\max} \leqslant \begin{cases} 1.95 \times 10^{-12} & (M_- = 1.5,\ 3,\ m^B/m^A = 0.5), \\ 4.35 \times 10^{-19} & (M_- = 1.5,\ 2,\ m^B/m^A = 0.25), \end{cases}$$

$$\hat{F}^B/(\hat{F}_-^B)_{\max} \leqslant \begin{cases} 1.62 \times 10^{-8} & (M_- = 1.5,\ m^B/m^A = 0.5,\ 0.25), \\ 1.10 \times 10^{-6} & (M_- = 3,\ m^B/m^A = 0.5), \\ 8.08 \times 10^{-7} & (M_- = 2,\ m^B/m^A = 0.25). \end{cases}$$

It is noted that the range in ζ_r is not truncated in our computation. On the other hand, the computational range in x_1 is $|x_1| \leqslant D$ $(= 17.7245 f_\delta)$ (cf. section 6.1). Let us introduce the following maximum difference between $\hat{F}^\alpha$ and $\hat{F}_+^\alpha$ and that between $\hat{F}^\alpha$ and $\hat{F}_-^\alpha$:

$$\big[\Delta \hat{F}^\alpha\big]_\pm = \max_{\zeta_1, \zeta_r} \big| \hat{F}^\alpha - \hat{F}_\pm^\alpha \big| / (\hat{F}_\pm^\alpha)_{\max}. \tag{82}$$

For $-D \leqslant x_1 < -14.5 f_\delta$,

$$\big[\Delta \hat{F}^\alpha\big]_- \leqslant \begin{cases} 3.31 \times 10^{-5} & (M_- = 1.5,\ 3,\ m^B/m^A = 0.5), \\ 2.60 \times 10^{-4} & (M_- = 1.5,\ m^B/m^A = 0.25), \\ 2.69 \times 10^{-5} & (M_- = 2,\ m^B/m^A = 0.25), \end{cases}$$

and for $14.5 f_\delta < x_1 \leqslant D$,

$$\left[\Delta \hat{F}^\alpha\right]_+ \leqslant \begin{cases} 1.88 \times 10^{-3} & (M_- = 1.5,\ 3,\ m^B/m^A = 0.5), \\ 2.67 \times 10^{-3} & (M_- = 1.5,\ 2,\ m^B/m^A = 0.25), \end{cases}$$

where x_1 is the original coordinate system.

Since the size of the present computation is quite large, we cannot perform the accuracy test in a more systematic way. However, concerning the accuracy of the collision integrals, we can obtain a measure of accuracy by computing the gain and loss terms numerically for Maxwellian distributions and comparing the result with the exact values. If we insert $\hat{F}^\alpha_-$ and $\hat{F}^\alpha_+$ in the RHS of equation (16), each collision term $\hat{G}^{\beta\alpha}[\hat{F}^\beta_\pm, \hat{F}^\alpha_\pm] - \hat{\nu}[\hat{F}^\beta_\pm]\hat{F}^\alpha_\pm$ vanishes, and therefore, we have

$$\hat{G}^{\beta\alpha}\left[\hat{F}^\beta_\pm, \hat{F}^\alpha_\pm\right] = \hat{\nu}\left[\hat{F}^\beta_\pm\right]\hat{F}^\alpha_\pm = \mathsf{F}^{\beta\alpha}_\pm(\zeta_1, \zeta_r). \tag{83}$$

The middle term $\hat{\nu}[\hat{F}^\beta_\pm]\hat{F}^\alpha_\pm$ can be calculated exactly and gives the exact $\mathsf{F}^{\beta\alpha}_\pm(\zeta_1, \zeta_r)$. On the other hand, the numerical values corresponding to the first and second terms, say $\hat{G}^{\beta\alpha}_{\pm jk}$ and $\hat{\nu}^{\beta\alpha}_{\pm jk}\hat{F}^\alpha_{\pm jk}$ $[\hat{F}^\alpha_{\pm jk} = \hat{F}^\alpha_\pm(\zeta_1^{(j)}, \zeta_r^{\alpha(k)})]$, can be computed from equations (50a) and (50b) and equation (54a) with $\hat{F}^{\alpha(n)}_{ijk} = \hat{F}^\alpha_{\pm jk}$. We compare $\hat{G}^{\beta\alpha}_{\pm jk}$ and $\hat{\nu}^{\beta\alpha}_{\pm jk}\hat{F}^\alpha_{\pm jk}$ with $\mathsf{F}^{\beta\alpha}_\pm(\zeta_1, \zeta_r)$ to get an estimate of the accuracy. In this check, if we compare the values only for a fixed ζ_r-lattice point $\zeta_r^{\alpha(k)}$, we need to construct the numerical kernels $\Omega^{\beta\alpha 0k}_{pqab}$ and $\Lambda^{\beta\alpha 0k}_{pa}$ only for the $\zeta_r^{\alpha(k)}$, so that a more variety of the lattice systems for the $\zeta_1\zeta_r$-plane can be checked. We consider the lattice systems ($\overline{\text{M5}}$), ($\overline{\text{M6}}$), (M7), and (M8) in *table III* in addition to ($\overline{\text{M1}}$), ($\overline{\text{M2}}$), (M3), and (M4). The bar on (M5), etc., has the same meaning as in ($\overline{\text{M1}}$) and ($\overline{\text{M2}}$). Let us introduce the following maximum difference relative to the maximum value of $\mathsf{F}^{\beta\alpha}_\pm$:

$$\mathsf{G}^{\beta\alpha}_\pm = \max_j \left|\hat{G}^{\beta\alpha}_{\pm jk} - \mathsf{F}^{\beta\alpha}_\pm(\zeta_1^{(j)}, \zeta_r^{\alpha(k)})\right| / \max_{\zeta_1} \mathsf{F}^{\beta\alpha}_\pm, \tag{84a}$$

$$\mathsf{L}^{\beta\alpha}_\pm = \max_j \left|\hat{\nu}^{\beta\alpha}_{\pm jk}\hat{F}^\alpha_{\pm jk} - \mathsf{F}^{\beta\alpha}_\pm(\zeta_1^{(j)}, \zeta_r^{\alpha(k)})\right| / \max_{\zeta_1} \mathsf{F}^{\beta\alpha}_\pm. \tag{84b}$$

In the case of $d^B_m/d^A_m = 1$ and $\chi^B_- = 0.1$, 0.5, 0.9, and 0.95, the $\mathsf{G}^{\beta\alpha}_\pm$ and $\mathsf{L}^{\beta\alpha}_\pm$ for $\zeta_r^{\alpha(k)} = \zeta_r^{\alpha(1)}$ [or $\zeta_r^{\alpha(k)} = \zeta_r^{(1)}$] (cf. *table III*) are estimated as follows:

$$\begin{aligned} &\mathsf{G}^{\beta\alpha}_\pm \leqslant 3.23 \times 10^{-4}, \qquad \mathsf{L}^{\beta\alpha}_\pm \leqslant 4.61 \times 10^{-5} \quad [\text{for } (\overline{\text{M1}})], \\ &\mathsf{G}^{\beta\alpha}_\pm \leqslant 3.98 \times 10^{-5}, \qquad \mathsf{L}^{\beta\alpha}_\pm \leqslant 6.31 \times 10^{-6} \quad [\text{for } (\overline{\text{M2}}),\ (\overline{\text{M5}}), \text{and } (\overline{\text{M6}})], \end{aligned}$$

for $M_- = 1.5$ and $m^B/m^A = 0.5$;

$$\begin{aligned} &\mathsf{G}^{\beta\alpha}_\pm \leqslant 3.93 \times 10^{-5}, \qquad \mathsf{L}^{\beta\alpha}_\pm \leqslant 5.28 \times 10^{-6} \quad [\text{for (M3)}], \\ &\mathsf{G}^{\beta\alpha}_\pm \leqslant 1.33 \times 10^{-4}, \qquad \mathsf{L}^{\beta\alpha}_\pm \leqslant 2.81 \times 10^{-4} \quad [\text{for (M7)}], \end{aligned}$$

for $M_- = 3$ and $m^B/m^A = 0.5$; and

$$\mathsf{G}^{\beta\alpha}_\pm \leqslant 3.93 \times 10^{-5}, \qquad \mathsf{L}^{\beta\alpha}_\pm \leqslant 5.28 \times 10^{-6} \quad [\text{for (M4) and (M8)}],$$

for $M_- = 1.5$ and 2 and $m^B/m^A = 0.25$.

7. Concluding remarks

In the present study, we have investigated the structure of a normal shock wave for a binary gas mixture on the basis of the Boltzmann equation for hard-sphere molecules. Extending the numerical kernel method developed in Ohwada [8] for a single component gas to the case of a binary mixture, we have constructed an accurate method to compute the collision integrals (sections 4.2 and 4.3). Then, we have analyzed the problem by an accurate finite-difference method in which the numerical kernel method is incorporated (section 4.1). As a result, the transition from the upstream to the downstream state was clarified for the velocity distribution functions as well as for the macroscopic variables (section 5). The accuracy of the computation was also examined carefully (section 6.3). The numerical kernels constructed in the present study can be applied to any problems in which the velocity distribution functions are of the form of equation (28).

In the present method, the collision integrals are approximated by using the values of the velocity distribution functions at the discrete lattice points in the molecular velocity space. One of the important mathematical questions relevant to this type of method is whether or not the approximated collision integrals converge to the real collision integrals of the Boltzmann equation when the lattice interval in the molecular velocity space tends to zero. For a single-component gas, a positive answer was given recently for some different types of discretization of the collision integral (Bobylev et al. [37], Rogier and Schneider [38], Panferov and Heintz [39]). In all of them, the discretization is made in such a way that the mass, momentum, and energy are conserved exactly in each collision. In this point, these conservative methods (or discrete velocity models) are different from the methods of Ohwada [8] and the present study, in which the conservation laws are not satisfied artificially but are satisfied approximately within the error of computation. In the latter methods, therefore, the conservation laws can be used as a measure of accuracy (see section 6.3).

The present computation was carried out on Fujitsu VPP800/63 computer at the Data Processing Center, Kyoto University, Fujitsu VPP800/12 computer at the Institute of Space and Astronautical Science, and VT-Alpha 533 and 600 Workstations at the Section of Dynamics in Aeronautics and Astronautics, Department of Aeronautics and Astronautics, Kyoto University.

Appendix A. Derivation of equations (53) and (54)

The Christoffel–Darboux formula (Abramowitz and Stegun [34]) for a system of orthonormal polynomials gives the following relation for the Laguerre polynomials:

$$(x-y)\sum_{s=0}^{H-1} L_s(x)L_s(y) = (c_{H-1,H-1}/c_{HH})\big[L_H(x)L_{H-1}(y) - L_H(y)L_{H-1}(x)\big]. \tag{A1}$$

Noting that $L_H(x) = c_{HH}\prod_{l=1}^{H}(x-y_l)$, where y_l are the zeros of $L_H(x)$, we put $y = y_k$ in equation (A1). Then, using the continuity of polynomials, we have

$$\prod_{l=1\ (\neq k)}^{H}(x-y_l) = \frac{1}{c_{H-1,H-1}L_{H-1}(y_k)}\sum_{l=0}^{H-1} L_l(y_k)L_l(x) \quad (k=1,\ldots,H), \tag{A2}$$

for all $x > 0$.

Now let us consider equation (44) with $H^\alpha = H$ and suppose that $\zeta_r^{\alpha(k)} = \sqrt{y_k/\hat{m}^\alpha}$ (or $\hat{m}^\alpha(\zeta_r^{\alpha(k)})^2 = y_k$) (equation (52)). For simplicity, let us put

$$\hat{m}^\alpha \zeta_r^2 \equiv x, \qquad \hat{F}_i^{\alpha(n)}(\zeta_1^{\alpha(j)}, \zeta_r) \exp\left(\frac{\hat{m}^\alpha \zeta_r^2}{2}\right) \equiv f_{ij}^\alpha(x),$$

$$\hat{F}_{ijk}^{\alpha(n)} \exp\left(\frac{\hat{m}^\alpha (\zeta_r^{\alpha(k)})^2}{2}\right) = \hat{F}_{ijk}^{\alpha(n)} \exp\left(\frac{y_k}{2}\right) \equiv f_{ijk}^\alpha.$$

Then, equation (44) is written as

$$f_{ij}^\alpha(x) = \sum_{l=0}^{H-1} a_{ijl}^{\alpha(n)} L_l(x). \tag{A3}$$

On the other hand, from the choice of $a_{ijl}^{\alpha(n)}$ (see equation (47) and the sentences below it), $f_{ij}^\alpha(x)$ is expressed as

$$f_{ij}^\alpha(x) = \sum_{k=1}^{H} f_{ijk}^\alpha \prod_{s=1\ (\neq k)}^{H} \frac{x - y_s}{y_k - y_s}. \tag{A4}$$

By equating the RHS's of (A3) and (A4) and using (A2), we obtain

$$\sum_{l=0}^{H-1} a_{ijl}^{\alpha(n)} L_l(x) = \sum_{k=1}^{H} f_{ijk}^\alpha \frac{1}{c_{H-1,H-1} L_{H-1}(y_k) \prod_{s=1\ (\neq k)}^{H} (y_k - y_s)} \sum_{s=0}^{H-1} L_s(y_k) L_s(x). \tag{A5}$$

If we integrate equation (A5) multiplied by $\exp(-x) L_m(x)$ with respect to x from 0 to infinity, we have, from the orthogonality relation (46), the following expression of $a_{ijm}^{\alpha(n)}$, i.e., equations (53a) and (53b):

$$a_{ijm}^{\alpha(n)} = \sum_{k=1}^{H} f_{ijk}^\alpha \frac{L_m(y_k)}{c_{H-1,H-1} L_{H-1}(y_k) \prod_{s=1\ (\neq k)}^{H} (y_k - y_s)}. \tag{A6}$$

By the use of (53a), equation (A3) is written as

$$f_{ij}^\alpha(x) = \sum_{l=0}^{H-1} \left(\sum_{k=1}^{H} w_{lk} \hat{F}_{ijk}^{\alpha(n)} \right) L_l(x). \tag{A7}$$

Using the expression $L_l(x) = \sum_{m=0}^{l} c_{ml} x^m$ and changing the order of summations, we obtain

$$f_{ij}^\alpha(x) = \sum_{m=0}^{H-1} \left(\sum_{k=1}^{H} \hat{F}_{ijk}^{\alpha(n)} \sum_{l=m}^{H-1} c_{ml} w_{lk} \right) x^m. \tag{A8}$$

The comparison of (A8) with (48) gives

$$A_{ijm}^{\alpha(n)} = \sum_{k=1}^{H} \hat{F}_{ijk}^{\alpha(n)} \sum_{l=m}^{H-1} c_{ml} w_{lk}, \tag{A9}$$

which is equivalent to equations (54a) and (54b).

Appendix B. Integration of equation (66b)

Let us introduce the following integral:

$$\tilde{\Theta}_a^{kl}(x_0, x_1, z, \theta, \bar{\epsilon}) = \int_{-\infty}^{\infty}\int_{-\infty}^{\infty} J_1^l U(J_1; x_0, x_1)\big(\sqrt{\hat{m}^\beta}\, J_r^{(k)}\big)^{2a} \exp\left(-\frac{(\sqrt{\hat{m}^\beta}\, J_r^{(k)})^2}{2}\right) \mathrm{d}w'\, \mathrm{d}w'', \tag{B1}$$

where

$$U(t; x_0, x_1) = \begin{cases} 1 & (x_0 < t < x_1), \\ 0 & (\text{otherwise}). \end{cases} \tag{B2}$$

Then, $\Theta_{pa}^k(z, \theta, \bar{\epsilon})$ in equation (66b) is expressed by a linear combination of $\tilde{\Theta}_a^{kl}(x_0, x_1, z, \theta, \bar{\epsilon})$ $(l = 0, 1, 2)$. For example, Θ_{1a}^k is expressed as follows:

$$\Theta_{1a}^k(z, \theta, \bar{\epsilon}) = \big[-\tilde{\Theta}_a^{k2}(0, 2h, z, \theta, \bar{\epsilon}) + 2h\tilde{\Theta}_a^{k1}(0, 2h, z, \theta, \bar{\epsilon})\big]/h^2. \tag{B3}$$

Therefore, the calculation of (66b) is reduced to that of (B1). The integration of (B1) can be carried out analytically and gives the following expression of $\tilde{\Theta}_a^{kl}$:

$$\begin{pmatrix} \tilde{\Theta}_a^{k2}(x_0, x_1, z, \theta, \bar{\epsilon}) \\ \tilde{\Theta}_a^{k1}(x_0, x_1, z, \theta, \bar{\epsilon}) \\ \tilde{\Theta}_a^{k0}(x_0, x_1, z, \theta, \bar{\epsilon}) \end{pmatrix} = \tilde{B}^k \begin{pmatrix} \tilde{Y}_a^{k2} \\ \tilde{Y}_a^{k1} \\ \tilde{Y}_a^{k0} \end{pmatrix}, \tag{B4}$$

where

$$\tilde{B}^k = \frac{1}{(\hat{m}^\beta)^2} \begin{pmatrix} \frac{\sin^2\theta}{\cos^3\theta} & 0 & 0 \\ 0 & \frac{\sin\theta}{\cos^2\theta} & 0 \\ 0 & 0 & \frac{1}{\cos\theta} \end{pmatrix} \begin{pmatrix} 1 & 2\zeta_r^{\alpha(k)}\cos\bar{\epsilon} & (\zeta_r^{\alpha(k)}\cos\bar{\epsilon})^2 \\ 0 & 1 & \zeta_r^{\alpha(k)}\cos\bar{\epsilon} \\ 0 & 0 & 1 \end{pmatrix} \begin{pmatrix} 1 & 2\sqrt{\hat{m}^\beta}\delta^{\beta\alpha}\frac{z}{\sin\theta} & \hat{m}^\beta\left(\delta^{\beta\alpha}\frac{z}{\sin\theta}\right)^2 \\ 0 & \sqrt{\hat{m}^\beta} & \hat{m}^\beta\delta^{\beta\alpha}\frac{z}{\sin\theta} \\ 0 & 0 & \hat{m}^\beta \end{pmatrix}, \tag{B5}$$

$$\delta^{\beta\alpha} = (\hat{m}^\beta - \hat{m}^\alpha)/(\hat{m}^\beta + \hat{m}^\alpha), \tag{B6}$$

$$\tilde{Y}_a^{kl} = \sum_{r=0}^{a} \binom{a}{r} \tilde{g}_{a-r} \times \tilde{q}_{2r+l}^k \quad (l = 0, 1, 2), \tag{B7}$$

$$\tilde{q}_s^k = E_s(\sqrt{\hat{m}^\beta}\, Z_1) - E_s(\sqrt{\hat{m}^\beta}\, Z_0), \tag{B8}$$

$$Z_i = x_i \cot\theta - \zeta_r^{\alpha(k)}\cos\bar{\epsilon} - \delta^{\beta\alpha}\frac{z}{\sin\theta} \quad (i = 0, 1). \tag{B9}$$

Here, $\binom{0}{0} = 1$; $E_s(x)$ is defined by

$$E_s(x) = \int_0^x t^s \exp(-t^2/2)\, \mathrm{d}t, \tag{B10}$$

and has the following recursion formula:

$$E_s(x) = -x^{s-1}\exp(-x^2/2) + (s-1)E_{s-2}(x),$$
$$E_0(x) = \sqrt{\pi/2}\,\mathrm{erf}(x/\sqrt{2}), \qquad E_1(x) = 1 - \exp(-x^2/2),$$

where

$$\mathrm{erf}(x) = \frac{2}{\sqrt{\pi}} \int_0^x \exp\bigl(-t^2\bigr)\,\mathrm{d}t, \tag{B11}$$

is the error function; and $\tilde{g}_s$ is defined by

$$\tilde{g}_s = \int_{-\infty}^{\infty} t^{2s} \exp\bigl(-t^2/2\bigr)\,\mathrm{d}t, \tag{B12}$$

namely,

$$\tilde{g}_s = (2s-1)(2s-3)\cdots 5\cdot 3\cdot 1\cdot \tilde{g}_0, \quad \tilde{g}_0 = \sqrt{2\pi}.$$

When $\beta = \alpha$, $\tilde{\Theta}_a^{kl}$ in equation (B1) does not depend on z because both of J_1 and $J_r^{(k)}$ are independent of z (cf. equations (64a) and (64b)). In this case, equations (B4)–(B9) are reduced to the following:

$$\begin{pmatrix} \tilde{\Theta}_a^{k2}(x_0, x_1, \theta, \bar{\epsilon}) \\ \tilde{\Theta}_a^{k1}(x_0, x_1, \theta, \bar{\epsilon}) \\ \tilde{\Theta}_a^{k0}(x_0, x_1, \theta, \bar{\epsilon}) \end{pmatrix} = \tilde{B}^k \begin{pmatrix} \tilde{Y}_a^{k2} \\ \tilde{Y}_a^{k1} \\ \tilde{Y}_a^{k0} \end{pmatrix}, \tag{B13}$$

$$\tilde{B}^k = \frac{1}{(\hat{m}^\alpha)^2} \begin{pmatrix} \frac{\sin^2\theta}{\cos^3\theta} & 0 & 0 \\ 0 & \frac{\sin\theta}{\cos^2\theta} & 0 \\ 0 & 0 & \frac{1}{\cos\theta} \end{pmatrix} \begin{pmatrix} 1 & 2\sqrt{\hat{m}^\alpha}\zeta_r^{\alpha(k)}\cos\bar{\epsilon} & \hat{m}^\alpha(\zeta_r^{\alpha(k)}\cos\bar{\epsilon})^2 \\ 0 & \sqrt{\hat{m}^\alpha} & \hat{m}^\alpha\zeta_r^{\alpha(k)}\cos\bar{\epsilon} \\ 0 & 0 & \hat{m}^\alpha \end{pmatrix}, \tag{B14}$$

$$\tilde{Y}_a^{kl} = \sum_{r=0}^{a} \binom{a}{r} \tilde{g}_{a-r} \times \tilde{q}_{2r+l}^k \quad (l = 0, 1, 2), \tag{B15}$$

$$\tilde{q}_s^k = E_s\bigl(\sqrt{\hat{m}^\alpha}\bigl(x_1\cot\theta - \zeta_r^{\alpha(k)}\cos\bar{\epsilon}\bigr)\bigr) - E_s\bigl(\sqrt{\hat{m}^\alpha}\bigl(x_0\cot\theta - \zeta_r^{\alpha(k)}\cos\bar{\epsilon}\bigr)\bigr). \tag{B16}$$

Appendix C. Integration of equation (66a)

Let us consider the following integral:

$$\begin{aligned} \tilde{\Gamma}_{ab}^{klm}(x_0, x_1, y_0, y_1, \theta, \bar{\epsilon}) = \sin\theta \int_0^\infty & z K_1^l U(K_1; x_0, x_1)\bigl(\sqrt{\hat{m}^\alpha}K_r^{(k)}\bigr)^{2b} \\ & \times \exp\biggl(-\frac{(\sqrt{\hat{m}^\alpha}K_r^{(k)})^2}{2}\biggr)\tilde{\Theta}_a^{km}(y_0, y_1, z, \theta, \bar{\epsilon})\,\mathrm{d}z. \end{aligned} \tag{C1}$$

Then, $\Gamma_{pqab}^k(\theta, \bar{\epsilon})$ in equation (66a) is expressed by a linear combination of $\tilde{\Gamma}_{ab}^{klm}$ $(l, m = 0, 1, 2)$. Therefore, the computation of Γ_{pqab}^k is reduced to that of $\tilde{\Gamma}_{ab}^{klm}$. The $\tilde{\Gamma}_{ab}^{klm}$ can be expressed in the following form.

$$\begin{pmatrix} \tilde{\Gamma}_{ab}^{k22} & \tilde{\Gamma}_{ab}^{k21} & \tilde{\Gamma}_{ab}^{k20} \\ \tilde{\Gamma}_{ab}^{k12} & \tilde{\Gamma}_{ab}^{k11} & \tilde{\Gamma}_{ab}^{k10} \\ \tilde{\Gamma}_{ab}^{k02} & \tilde{\Gamma}_{ab}^{k01} & \tilde{\Gamma}_{ab}^{k00} \end{pmatrix} = \tilde{A}^k \begin{pmatrix} \tilde{X}_{ab}^{k32} & \tilde{X}_{ab}^{k31} & \tilde{X}_{ab}^{k30} \\ \tilde{X}_{ab}^{k22} & \tilde{X}_{ab}^{k21} & \tilde{X}_{ab}^{k20} \\ \tilde{X}_{ab}^{k12} & \tilde{X}_{ab}^{k11} & \tilde{X}_{ab}^{k10} \\ \tilde{X}_{ab}^{k02} & \tilde{X}_{ab}^{k01} & \tilde{X}_{ab}^{k00} \end{pmatrix}, \tag{C2}$$

where

$$\tilde{A}^k = \frac{1}{(\hat{\mu}^{\beta\alpha})^2}\exp\left(-\frac{\hat{m}^\alpha(\zeta_r^{\alpha(k)}\sin\bar{\epsilon})^2}{2}\right)\begin{pmatrix}\frac{\cos^2\theta}{\sin^3\theta} & 0 & 0\\ 0 & \frac{\cos\theta}{\sin^2\theta} & 0\\ 0 & 0 & \frac{1}{\sin\theta}\end{pmatrix}$$
$$\times\begin{pmatrix}1 & -3\sqrt{\hat{m}^\alpha}\zeta_r^{\alpha(k)}\cos\bar{\epsilon} & 3\hat{m}^\alpha(\zeta_r^{\alpha(k)}\cos\bar{\epsilon})^2 & -(\hat{m}^\alpha)^{3/2}(\zeta_r^{\alpha(k)}\cos\bar{\epsilon})^3\\ 0 & \sqrt{\hat{m}^\alpha} & -2\hat{m}^\alpha\zeta_r^{\alpha(k)}\cos\bar{\epsilon} & (\hat{m}^\alpha)^{3/2}(\zeta_r^{\alpha(k)}\cos\bar{\epsilon})^2\\ 0 & 0 & \hat{m}^\alpha & -(\hat{m}^\alpha)^{3/2}\zeta_r^{\alpha(k)}\cos\bar{\epsilon}\end{pmatrix}, \tag{C3}$$

$$\tilde{X}_{ab}^{klm} = \sum_{r=0}^{b}\binom{b}{r}\left(\sqrt{\hat{m}^\alpha}\zeta_r^{\alpha(k)}\sin\bar{\epsilon}\right)^{2r}\times\tilde{p}_{a,2(b-r)+l}^{km}\quad(l=0,1,2,3;\ m=0,1,2), \tag{C4}$$

$$\tilde{p}_{as}^{km} = \int_{\sqrt{\hat{m}^\alpha}Z_0}^{\sqrt{\hat{m}^\alpha}Z_1}\bar{z}^s\exp(-\bar{z}^2/2)\tilde{\Theta}_a^{km}(y_0,y_1,z,\theta,\bar{\epsilon})\,\mathrm{d}\bar{z}, \tag{C5}$$

$$z = \frac{\hat{m}^\alpha}{\hat{\mu}^{\beta\alpha}\sin\theta}\left(\frac{\bar{z}}{\sqrt{\hat{m}^\alpha}} - \zeta_r^{\alpha(k)}\cos\bar{\epsilon}\right), \tag{C6}$$

$$Z_i = x_i\tan\theta + \zeta_r^{\alpha(k)}\cos\bar{\epsilon}\quad(i=0,1). \tag{C7}$$

The integration with respect to $\bar{z}$ in (C5) is carried out numerically. Then, the double integral with respect to $\bar{\epsilon}$ and θ in (65) is computed numerically.

When $\beta=\alpha$, equation (C1) is reduced to the following form, since $\tilde{\Theta}_a^{km}$ is independent of z.

$$\tilde{\Gamma}_{ab}^{klm}(x_0,x_1,y_0,y_1,\theta,\bar{\epsilon}) = \tilde{\Gamma}_b^{kl}(x_0,x_1,\theta,\bar{\epsilon})\times\tilde{\Theta}_a^{km}(y_0,y_1,\theta,\bar{\epsilon}), \tag{C8}$$

where

$$\tilde{\Gamma}_b^{kl}(x_0,x_1,\theta,\bar{\epsilon}) = \sin\theta\int_0^\infty z K_1^l U(K_1;x_0,x_1)\left(\sqrt{\hat{m}^\alpha}K_r^{(k)}\right)^{2b}\exp\left(-\frac{(\sqrt{\hat{m}^\alpha}K_r^{(k)})^2}{2}\right)\mathrm{d}z. \tag{C9}$$

We can carry out this integration analytically to obtain the following expression of $\tilde{\Gamma}_b^{kl}$:

$$\begin{pmatrix}\tilde{\Gamma}_b^{k2}(x_0,x_1,\theta,\bar{\epsilon})\\ \tilde{\Gamma}_b^{k1}(x_0,x_1,\theta,\bar{\epsilon})\\ \tilde{\Gamma}_b^{k0}(x_0,x_1,\theta,\bar{\epsilon})\end{pmatrix} = \tilde{A}^k\begin{pmatrix}\tilde{X}_b^{k3}\\ \tilde{X}_b^{k2}\\ \tilde{X}_b^{k1}\\ \tilde{X}_b^{k0}\end{pmatrix}, \tag{C10}$$

$$\tilde{X}_b^{kl} = \sum_{r=0}^{b}\binom{b}{r}\left(\sqrt{\hat{m}^\alpha}\zeta_r^{\alpha(k)}\sin\bar{\epsilon}\right)^{2r}\times\tilde{p}_{2(b-r)+l}^{k}\quad(l=0,1,2,3), \tag{C11}$$

$$\tilde{p}_s^k = E_s\left(\sqrt{\hat{m}^\alpha}Z_1\right) - E_s\left(\sqrt{\hat{m}^\alpha}Z_0\right), \tag{C12}$$

$$Z_i = x_i\tan\theta + \zeta_r^{\alpha(k)}\cos\bar{\epsilon}\quad(i=0,1). \tag{C13}$$

Here, $\tilde{A}^k$ is given by equation (C3) with $\hat{\mu}^{\beta\alpha}=\hat{m}^\alpha$. With this expression of $\tilde{\Gamma}_b^{kl}$, we carry out the double integration with respect to $\bar{\epsilon}$ and θ in (65) numerically.

Acknowledgement

This work was partially supported by the grants-in-aid (No. 00114103 and No. 10045040) for Scientific Research from the Ministry of Education, Science, Sports and Culture in Japan.

References

[1] Mott-Smith H.M., The solution of the Boltzmann equation for a shock wave, Phys. Rev. 2nd Ser. 82 (1951) 885.
[2] Liepmann H.W., Narashimha R., Chahine M.T., Structure of a plane shock layer, Phys. Fluids 5 (1962) 1313.
[3] Bird G.A., Aspects of the structure of strong shock waves, Phys. Fluids 13 (1970) 1172.
[4] Cercignani C., The Boltzmann Equation and Its Applications, Chap. VII, Springer, Berlin, 1988.
[5] Fiszdon W., The structure of plane shock waves, in: Fiszdon W. (Ed.), Rarefied Gas Flows: Theory and Experiment, Springer, Vienna, 1981, p. 447.
[6] Bird G.A., Molecular Gas Dynamics and the Direct Simulation of Gas Flows, Oxford Univ. Press, Oxford, 1994.
[7] Cercignani C., Frezzotti A., Grosfils P., The structure of an infinitely strong shock wave, Phys. Fluids 11 (1999) 2757.
[8] Ohwada T., Structure of normal shock waves: Direct numerical analysis of the Boltzmann equation for hard-sphere molecules, Phys. Fluids A 5 (1993) 217.
[9] Sone Y., Ohwada T., Aoki K., Temperature jump and Knudsen layer in a rarefied gas over a plane wall: Numerical analysis of the linearized Boltzmann equation for hard-sphere molecules, Phys. Fluids A 1 (1989) 363.
[10] Ohwada T., Sone Y., Aoki K., Numerical analysis of the shear and thermal creep flows of a rarefied gas over a plane wall on the basis of the linearized Boltzmann equation for hard-sphere molecules, Phys. Fluids A 1 (1989) 1588.
[11] Ohwada T., Sone Y., Analysis of thermal stress slip flow and negative thermophoresis using the Boltzmann equation for hard-sphere molecules, Eur. J. Mech. B-Fluids 11 (1992) 389.
[12] Ohwada T., Sone Y., Aoki K., Numerical analysis of the Poiseuille and thermal transpiration flows between two parallel plates on the basis of the Boltzmann equation for hard-sphere molecules, Phys. Fluids A 1 (1989) 2042.
[13] Sone Y., Takata S., Ohwada T., Numerical analysis of the plane Couette flow of a rarefied gas on the basis of the linearized Boltzmann equation for hard-sphere molecules, Eur. J. Mech. B-Fluids 9 (1990) 273.
[14] Takata S., Sone Y., Aoki K., Numerical analysis of a uniform flow of a rarefied gas past a sphere on the basis of the Boltzmann equation for hard-sphere molecules, Phys. Fluids A 5 (1993) 716.
[15] Sone Y., Takata S., Wakabayashi M., Numerical analysis of a rarefied gas flow past a volatile particle using the Boltzmann equation for hard-sphere molecules, Phys. Fluids 6 (1994) 1914.
[16] Takata S., Sone Y., Flow induced around a sphere with a non-uniform surface temperature in a rarefied gas, with application to the drag and thermal force problems of a spherical particle with an arbitrary thermal conductivity, Eur. J. Mech. B-Fluids 14 (1995) 487.
[17] Ohwada T., Numerical analysis of normal shock waves on the basis of the Boltzmann equation for hard-sphere molecules, in: Shizgal B.D., Weaver D.P. (Eds.), Rarefied Gas Dynamics: Theory and Simulations, AIAA, Washington, D.C., 1994, p. 482.
[18] Ohwada T., Heat flow and temperature and density distributions in a rarefied gas between parallel plates with different temperatures: Finite difference analysis of the nonlinear Boltzmann equation for hard-sphere molecules, Phys. Fluids 8 (1996) 2153.
[19] Ohwada T., Investigation of heat transfer problem of a rarefied gas between parallel plates with different temperatures, in: Shen C. (Ed.), Rarefied Gas Dynamics, Peking University Press, Beijing, 1997, p. 327.
[20] Center R.E., Measurement of shock-wave structure in Helium-Argon mixtures, Phys. Fluids 10 (1967) 1777.
[21] Harnett L.N., Muntz E.P., Experimental investigation of normal shock wave velocity distribution functions in mixtures of Argon and Helium, Phys. Fluids 15 (1972) 565.
[22] Gmurczyk A.S., Tarczyński M., Walenta Z.A., Shock wave structure in the binary mixtures of gases with disparate molecular masses, in: Campargue R. (Ed.), Rarefied Gas Dynamics, Commissariat a l'Energie Atomique, Paris, Vol. 1, 1979, p. 333.
[23] Oberai M.M., A Mott-Smith distribution to describe the structure of a plane shock wave in a binary mixture, Phys. Fluids 9 (1966) 1634.
[24] Oberai M.M., Sinha U.N., Shock wave structure in binary gas mixture, in: Becker M., Fiebig M. (Eds.), Rarefied Gas Dynamics, DFVLR, Povz-Wahn, Vol. 1, 1974, B. 25.
[25] Beylich A.E., Kinetic model for the shock structure in a binary gas mixture, Phys. Fluids 11 (1968) 2764.
[26] Fernández-Feria R., Fernández de la Mora J., Shock wave structure in gas mixtures with large mass disparity, J. Fluid Mech. 179 (1987) 21.
[27] Abe K., Oguchi H., Shock wave structures in binary gas mixtures with regard to temperature overshoot, Phys. Fluids 17 (1974) 1333.
[28] Hamel B.B., Disparate mass mixture flows, in: Potter J.L. (Ed.), Rarefied Gas Dynamics, AIAA, New York, Vol. 1, 1977, p. 171.
[29] Bird G.A., The structure of normal shock waves in a binary gas mixture, J. Fluid Mech. 31 (1968) 657.
[30] Bird G.A., Shock wave structure in gas mixtures, in: Oguchi H. (Ed.), Rarefied Gas Dynamics, University of Tokyo Press, Tokyo, Vol. 1, 1984, p. 175.
[31] Raines A.A., Conservative method of evaluation of Boltzmann collision integrals for cylindrical symmetry, in: Brun R., Campargue R., Gatignol R., Lengrand J.-C. (Eds.), Rarefied Gas Dynamics, Cépaduès-Éditions, Toulouse, Vol. 2, 1999, p. 173.
[32] Kogan M.N., Rarefied Gas Dynamics, Plenum, New York, 1969.

[33] Chapman S., Cowling T.G., The Mathematical Theory of Non-Uniform Gases, 3rd ed., Cambridge University Press, London, 1970.
[34] Abramowitz M., Stegun I.A., Handbook of Mathematical Functions, Dover, New York, 1965, Chap. 22.
[35] Ralston A., Rabinowitz P., A First Course in Numerical Analysis, 2nd ed., McGraw-Hill, New York, 1978, Chap. 4.
[36] Garzó V., Santos A., Brey J.J., A kinetic model for a multicomponent gas, Phys. Fluids A 1 (1989) 380.
[37] Bobylev A.V., Palczewski A., Schneider J., A consistency result for a discrete velocity model of the Boltzmann equation, SIAM J. Numer. Anal. 34 (1997) 1865.
[38] Rogier F., Schneider J., A direct method for solving the Boltzmann equation, Transp. Ther. Stat. Phys. 23 (1994) 313.
[39] Panferov V., Heintz A., A new consistent discrete-velocity model for the Boltzmann equation, Math. Method. Appl. Sci. (2000) (accepted for publication).